

Horizon crossing causes baryogenesis, magnetogenesis and dark-matter acoustic wave

She-Sheng Xue*

ICRANet, Piazzale della Repubblica, 10-65122, Pescara,

Physics Department, Sapienza University of Rome, P.le A. Moro 5, 00185, Rome, Italy

Spacetime \mathcal{S} produces massive particle-antiparticle pairs $\bar{F}F$ that in turn annihilate to spacetime. Such back and forth gravitational process $\mathcal{S} \Leftrightarrow \bar{F}F$ is described by Boltzmann-type cosmic rate equation of pair-number conservation. This cosmic rate equation, Einstein equation, and the reheating equation of pairs decay to relativistic particles completely determine the horizon H , cosmological energy density, massive pair and radiation energy densities in reheating epoch. Moreover, oscillating $\mathcal{S} \Leftrightarrow \bar{F}F$ process leads to the acoustic perturbations of massive particle-antiparticle symmetric and asymmetric densities. We derive wave equations for these perturbations and find frequencies of lowest lying modes. Comparing their wavelengths with horizon variation, we show their subhorizon crossing at preheating, and superhorizon crossing at reheating. The superhorizon crossing of particle-antiparticle asymmetric perturbations accounts for the baryogenesis of net baryon numbers, whose electric currents lead to magnetogenesis. The baryon number-to-entropy ratio, upper and lower limits of primeval magnetic fields are computed in accordance with observations. Given a pivot comoving wavelength, it is shown that these perturbations, as dark-matter acoustic waves, originate in pre-inflation and return back to the horizon after the recombination, possibly leaving imprints on the matter power spectrum at large length scales. Due to the Jeans instability, tiny pair-density acoustic perturbations in superhorizon can be amplified to the order of unity. Thus their amplitudes at reentry horizon become non-linear and maintain approximately constant physical sizes, and have physical influences on the formation of large scale structure and galaxies.

PACS numbers:

Keywords:

*Electronic address: xue@icra.it; shesheng.xue@gmail.com

Contents

I. Introduction	4
II. Einstein equation and pair production	6
A. Generalized equation for the Friedmann Universe	6
B. Particle-antiparticle pair production from spacetime	7
C. Naturally resultant inflation and CMB observations	8
III. Cosmic rate equation for pairs and spacetime	9
A. Particle-antiparticle pair annihilation and decay	9
B. Boltzmann rate equation for particle-antiparticle pairs and spacetime	10
C. A close set of fundamental equations in the reheating epoch	11
IV. Different episodes in the reheating epoch	12
A. preheating episode: <i>P-episode</i>	13
B. Massive pairs domination: <i>M-episode</i>	13
C. Relativistic particles domination: <i>R-episode</i> of the genuine reheating	15
V. Particle and antiparticle oscillating perturbations	16
A. Particle density perturbations	16
1. Continuum and Eulerian equations of particles	17
2. Density perturbations of particles and antiparticles	17
B. Symmetric and asymmetric density perturbations	18
1. Acoustic wave equations for density perturbations	18
2. Oscillating equations of lowest lying modes	19
VI. Particle-antiparticle asymmetry and horizon crossing	20
A. Under- and over-damped oscillating modes and horizon crossing	20
1. Under- and over-damped oscillating modes	21
2. Lowest lying mode crossing horizon	21
B. Symmetric and asymmetric oscillating amplitudes at horizon crossing	22
1. Lowest lying mode amplitudes at horizon crossing	23
2. Particle-antiparticle asymmetry due to horizon crossing	23
VII. Horizon crossings at reheating start and end	24

A. Subhorizon crossing in preheating \mathcal{P} -episode	25
1. Particle-antiparticle asymmetry in pre-inflation and inflation	25
2. Particle-antiparticle symmetry in \mathcal{M} -episode	25
3. Subhorizon crossing and particle-antiparticle symmetry	26
B. Superhorizon crossing in genuine reheating \mathcal{R} -episode	28
1. Superhorizon crossing in genuine reheating \mathcal{R} -episode	28
2. Initial particle-antiparticle asymmetry for standard cosmology	29
VIII. Baryogenesis and magnetogenesis in reheating epoch	31
A. Origin of net baryon numbers	31
B. Baryon number-to-entropy ratio	32
C. Magnetogenesis via baryogenesis	32
1. Upper limit of primordial magnetic fields	33
2. Lower limit of primordial magnetic fields	34
IX. Dark-matter acoustic wave and large-scale structure	35
A. Pair-density and particle-antiparticle-density perturbations	36
B. Pair-density perturbation and large-scale structure	37
1. Stable modes and dark-matter sound waves	38
2. Unstable modes and large-scale structure	39
C. Particle-antiparticle density perturbations and “plasma” acoustic wave	41
X. Summary and remarks	42
XI. Acknowledgment	44
References	44

I. INTRODUCTION

In the standard model of modern cosmology (Λ CDM), the cosmological constant, inflation, reheating, dark matter and coincidence problem have been long standing basic issues since decades. The inflation [1] is a fundamental epoch and the reheating [2] is a critical mechanism, which transition the Universe from the cold massive state left by inflation to the hot Big Bang [3]. The cosmic microwave background (CMB) observations have been attempting to determine a unique model of inflation and reheating.

In addition, the baryon and anti-baryon asymmetry is observed with the baryon number-to-entropy ratio $n_B/s = 0.864_{-0.015}^{+0.016} \times 10^{-10}$ [4]. We recall that in the Standard Model of elementary particle physics, it is difficult to have baryogenesis, and a number of ideas and efforts for the generation of baryon asymmetry with ingredients from beyond the Standard Model (SM), have been proposed [5]. Moreover, some interesting connections between reheating and baryogenesis have been studied [6]. Moreover, magnetic fields have been observed in galaxies $B_{10-10^2\text{kpc}} \sim 10^{-5}\text{G}$ and galaxy clusters $B_{0.1-1\text{Mpc}} \sim 10^{-6}\text{G}$. There is a (conservative) lower bound on the strength of magnetic fields with cosmic scale correlation lengths $B_{>1\text{Mpc}} > 10^{-17}\text{G}$, see Ref. [7]. On the other hand, CMB observations have put upper bounds on it $B_{1\text{Mpc}}^{\text{prim}} < 10^{-9}\text{G}$ [8]. Many ideas and efforts have been put forth to understand the the primordial origin of these magnetic fields [9, 10]

On the other hand, what is the crucial role that the cosmological Λ term play in inflation and reheating, and what is the essential reason for the coincidence of dark-matter dominate matter density and the cosmological Λ energy density. There are various models and many efforts, that have been made to approach these issues, and readers are referred to review articles and professional books, for example, see Refs. [11–30].

Suppose that the quantum gravity originates the cosmological term $\Lambda \sim M_{\text{pl}}^2$ at the Planck scale. The initial state of Universe is an approximate de Sitter spacetime of the horizon $H_o \approx (\Lambda/3)^{1/2}$ without any matter. The cosmological Λ energy density drives the spacetime inflation with the scale factor $a(t) \approx e^{H_o t}$. On the other hand, de Sitter spacetime is unstable against spontaneous particle creations [31, 32]. The cosmological energy density ρ_Λ drives inflation and simultaneously reduces its value to create the pair-energy density ρ_M via the continuous pair productions of massive fermions and antifermions $m \sim M_{\text{pl}}$ for matter content. The decreasing ρ_Λ and increasing ρ_M , in turn, slows down the inflation to its end when the pair production rate Γ_M is larger than the Hubble rate H of inflation. This leads to a natural inflation, whose $r-n_s$ relation in terms of the inflation e -folding number $N_{\text{end}} = 50, 60$ agrees with the constrains from CMB measurements [33].

A large number of massive pairs is produced and reheating epoch starts. In addition to Einstein equation and energy-conservation law, we introduce the Boltzmann-type cosmic rate equation (20) describing the number of pairs produced from (annihilating to) the spacetime, and reheating equation describing massive unstable pairs decay to relativistic particles and thermodynamic laws. This forms a close set of four independent differential equations uniquely determining H , ρ_Λ , ρ_M and radiation-energy density ρ_R , given the initial conditions at inflation end. Numerical solutions demonstrate three episodes of preheating, massive pairs dominate and genuine reheating. Results show that ρ_Λ can efficiently converts to ρ_M by producing massive pairs, whose decay accounts for reheating ρ_R , temperature and entropy of the Big-Bang Universe. As a result, the obtained inflation e -folding number, reheating scale, temperature and entropy are in terms of the tensor-to-scalar ratio in the theoretically predicated range $0.042 \lesssim r \lesssim 0.048$, consistently with current observations [34].

Above studies provide us the knowledges in particular how the horizon H varies and pairs oscillate $\mathcal{S} \Leftrightarrow \bar{F}F$ in the reheating epoch. These oscillations cause particle-antiparticle symmetric and asymmetric perturbations, whose superhorizon crossings accounts for baryogenesis, magnetogenesis and dark-matter acoustic wave. We try to present detailed studies as follow. In Sec. II, we briefly summarise the fundamental equations used: (i) two independent equations of Friedmann and energy conservation law; (ii) the pair-production number density and rate, and previous results obtained for pre-inflation and inflation epochs. In Sec. III, we discuss the back and forth process $\mathcal{S} \Leftrightarrow \bar{F}F$ and cosmic rate equation determining the relation between the matter density ρ_M in the Einstein equations and the pair density $\rho_M^H(H)$ produced by the pair-production process. In Secs. IV, we briefly recall the three episodes of reheating epoch. We describe the particle-antiparticle symmetric and asymmetric density perturbations, and derive their acoustic wave equations in Secs. V. We analyse their acoustic wavelengths in Sec. VI and discuss their horizon crossings that cause the particle-antiparticle asymmetry in Sec. VII. The resultant baryogenesis and magnetogenesis in the reheating are shown and the baryon number-to-entropy ratio and primeval magnetic field are calculated In Secs. VIII and VIII C. The studies of the dark-matter acoustic waves for a given comoving wavelength and their relevances to physical observations and effects at large distance scales are presented in Sec. IX. The article ends with a brief summary of results and remarks.

In this article, $G = M_{\text{pl}}^{-2}$ is the the Newton constant, M_{pl} is the Planck scale and reduced Planck scale $m_{\text{pl}} \equiv (8\pi)^{-1/2}M_{\text{pl}} = 2.43 \times 10^{18}\text{GeV}$.

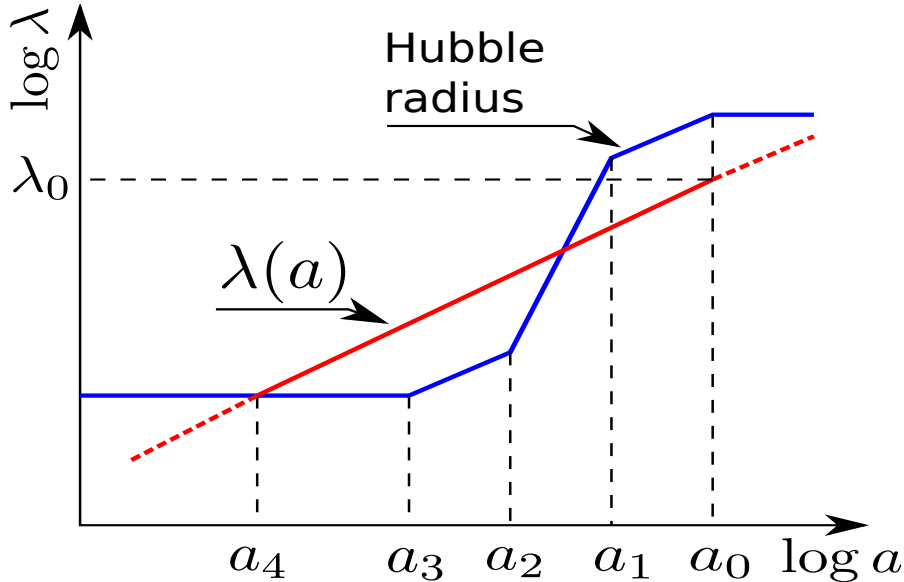


FIG. 1: This figure is duplicated from Fig. 1 in Ref. [35]. Schematic evolution of the Hubble radius H^{-1} and the physical length scale $\lambda(a)$, where physically interested scale $\lambda_0 = \lambda(a_0)$ at the present time $a_0 = 1$ crossed the Hubble horizon at the early time a_4 . Setting the scale factor $a_4 = a_*$ at the inflation scale H_*^{-1} fixed by the CMB pivot scale $\lambda_0 = \lambda_* = k_*^{-1}$. The pre-inflation $a > a_*$, the inflation $a_4 < a < a_3 = a_{\text{end}}$ and the inflation end $a_3 = a_{\text{end}}$, the reheating $a_3 < a < a_2 = a_R$, the genuine reheating at a_R and the recombination at $a_1 = a_{\text{eq}}$.

II. EINSTEIN EQUATION AND PAIR PRODUCTION

To proceed more detailed discussions and calculations on the reheating epoch, for readers' convenience, we present the brief and necessary summaries of the scenario $\tilde{\Lambda}$ CDM and its applications to the pre-inflation and inflation epochs.

A. Generalized equation for the Friedmann Universe

The Universe evolution from the inflation to the reheating is rather complex. In order to study the different episodes of the reheating epoch after the inflation, we rewrite the generalised equations for the Friedmann Universe as [34],

$$H^2 = (3m_{\text{pl}}^2)^{-1}(\rho_\Lambda + \rho_M + \rho_R), \quad (1)$$

$$\dot{H} = -(3/2)(3m_{\text{pl}}^2)^{-1}[(1 + \omega_M)\rho_M + (1 + \omega_R)\rho_R]. \quad (2)$$

where the Hubble rate $H \equiv \dot{a}/a$ of the scale factor $a(t)$ variation and $\dot{H} \equiv dH/dt$. The energy density ρ_M is a specific notation for massive pairs of $\omega_M \approx 0$. The energy density ρ_R a specific

notation for relativistic particles of $\omega_R \approx 1/3$. Their Equations of States are defined as $\omega_{M,R} = p_{M,R}/\rho_{M,R}$ and $p_{M,R}$ is the pressure of massive pairs or relativistic particles respectively. The energy density $\rho_\Lambda \equiv \Lambda^2/(8\pi G)$ and $\omega_\Lambda \equiv -1$ are attributed to the cosmological Λ -term.

Moreover, we introduce the expanding time scale τ_H and the ϵ -rate representing the rate of the H variation in time:

$$\tau_H \equiv H^{-1}; \quad \epsilon \equiv -\frac{\dot{H}}{H^2} = \frac{3\rho_M + (4/3)\rho_R}{2\rho_\Lambda + \rho_M + \rho_R}, \quad (3)$$

whose values characterise different epochs in Universe evolution. Note that in the inflation epoch the ϵ -rate is analogous to the so-called slow-roll parameter. As a convenient unit for calculations and expressions, we adopt the reduced Planck scale $m_{\text{pl}} \equiv (8\pi G)^{-1/2} = 1$, unless otherwise stated. In order to illustrate the pre-inflation, inflation and different episodes of the reheating epoch studied in this article, a schematic description of the Universe evolution for the standard cosmological scenario is presented in Fig. 1.

B. Particle-antiparticle pair production from spacetime

In this section, we briefly recall how to calculate the energy density ρ_M^H of the matter produced from the spacetime horizon H by the pair production of particles F and antiparticles \bar{F} :

$$\mathcal{S} \Rightarrow F + \bar{F}, \quad (4)$$

where \mathcal{S} indicates the spacetime. Such pair production is considered to be a semi-classical process of producing particles and antiparticles in the slowly time-varying horizon H . In the physical regime, where produced F and \bar{F} particle masses m are much larger than the horizon H ($m/H \gg 1$), i.e., they are well inside the horizon, we approximately obtain the averaged number, mass densities and pressure of massive pairs produced from $t = 0$ to $t \gtrsim 2\pi H^{-1}$ [33],

$$\rho_M^H \approx 2\chi m^2 H^2 (1 + s), \quad (5)$$

$$p_M^H \approx (s/3)\rho_M^H, \quad s \approx 1/2(H/m)^2 \ll 1 \quad (6)$$

$\omega_M = p_M/\rho_M \approx s/3$, the pair number density $n_M^H \approx \rho_M^H/(2m)$ and pair-production rate

$$\Gamma_M \approx -(\chi m/4\pi)(H^{-1}dH/dx) = (\chi m/4\pi)\epsilon, \quad (7)$$

where the theoretical coefficient $\chi \approx 1.85 \times 10^{-3}$ and the effective mass parameter m represents the mass and degeneracy of pairs.

C. Naturally resultant inflation and CMB observations

In the pair-production process, the cosmological term ρ_Λ and the horizon H must decrease, because the gravitational energy of the spacetime has to pay for the energy gain due to massive pair production and pairs' kinetic energy. This back reaction of pair productions on the spacetime has been taken into account by the Einstein equation (1) and generalised conservation law (2).

As indicated in Fig. 1, the pre-inflation epoch ($a < a_4$) when $H \gg \Gamma_M$, the inflation epoch ($a_4 \leq a \leq a_3$) when $H > \Gamma_M$, $\rho_\Lambda \gg \rho_M$, $\rho_R \approx 0$, and $\epsilon \approx (3/2)\rho_M/\rho_\Lambda \ll 1$. Using $\rho_M \approx \rho_M^H$ (5) and Eq. (2), we obtain the slowly decreasing

$$H = H_* e^{-\chi m_*^2 x} = H_* e^{-\chi m_*^2 N} \quad (8)$$

in terms of the e -folding variable $x = \ln(a/a_*) = N$. The m_* is the mass parameter in the inflation epoch. The initial scale H_* corresponds to the interested mode of the pivot scale k_* crossed the horizon ($k_* = H_* a_*$) for CMB power spectra observations: the spectral index $n_s \approx 0.965$ and the scalar amplitude $A_s = \Delta_{\mathcal{R}}^2 \approx 2.1 \times 10^{-9}$ at $k_* = 0.05 \text{ (Mpc)}^{-1}$ [36]. As a result, we determine the mass parameter m_* and ϵ -rate value ϵ^* ($n_s = 1 - 2\epsilon^*$) at the inflation scale H_*

$$m_* \approx 3.08 m_{\text{pl}}, \quad \epsilon^* = \chi m_*^2 \approx 1.75 \times 10^{-2}, \quad (9)$$

$$H_* = 3.15 \times 10^{-5} (r/0.1)^{1/2} m_{\text{pl}}, \quad (10)$$

where r is the scalar-tensor-ratio and the dimensionless notation $\chi m_*^2 \equiv \chi(m_*/m_{\text{pl}})^2$ for $m_{\text{pl}} = 1$ is used. The energy-density ratio of pairs and cosmological term is given by

$$\frac{\rho_M^*}{\rho_\Lambda^*} \approx \frac{2\chi(m_* H_*)^2}{3(m_{\text{pl}} H_*)^2} = \frac{2}{3} \chi m_*^2 \approx 1.17 \times 10^{-2}, \quad (11)$$

and $H_*^2 \approx \rho_\Lambda^*/(3m_{\text{pl}}^2)$.

The transition from the inflation epoch $H > \Gamma_M$ to the reheating epoch $\Gamma_M > H$ is physically continuous. We can estimate the inflation ending scale H_{end} by using $H_{\text{end}} \lesssim \Gamma_M$. From Eq. (8), the inflation ending scale H_{end} is

$$\begin{aligned} H_{\text{end}} &= H_* e^{-\chi m_*^2 N_{\text{end}}} \\ &\approx H_* e^{-(1-n_s)N_{\text{end}}/2} \approx (0.42, 0.35) H_*, \end{aligned} \quad (12)$$

for the e -folding number $N_{\text{end}} = (50, 60)$ and the tensor-to-scalar ratio $r = (0.037, 0.052)$, the $r-n_s$ relation was shown in accordance with the constraints from CMB measurements.

Equations (10,11,12), $\chi \ll 1$ and $\epsilon^* \ll 1$ (9) show that the H -variation is very small in the inflation epoch, implying

$$H_{\text{end}}^2 = \frac{\rho_{\Lambda}^{\text{end}} + \rho_M^{\text{end}}}{3m_{\text{pl}}^2} \gtrsim \frac{\rho_{\Lambda}^{\text{end}}}{3m_{\text{pl}}^2}; \quad \frac{\rho_M^{\text{end}}}{\rho_{\Lambda}^{\text{end}}} \ll 1, \quad (13)$$

namely, the cosmological term $\rho_{\Lambda}^{\text{end}} \approx 3m_{\text{pl}}^2 H_{\text{end}}^2$ is still dominant over the pair energy density $\rho_M^{\text{end}} \approx 2\chi m_*^2 H_{\text{end}}^2$ at the inflation end. We consider the ratio $\rho_M^{\text{end}}/\rho_{\Lambda}^{\text{end}}$ (11) and the scale H_{end} (12) as initial conditions of the reheating epoch ($a_3 \leq a \leq a_2$ in Fig. 1) to be studied in Sec. IV.

III. COSMIC RATE EQUATION FOR PAIRS AND SPACETIME

The inflation epoch ends and reheating epoch starts. The transitioning process from one to another cannot be instantaneous and must be very complex, due to the large density of particle-antiparticle pairs and the back reactions of microscopic and macroscopic processes. One of them is that pairs annihilate back to the spacetime, in addition to they are produced from the spacetime. This means that the produced pairs' energy density ρ_M^H is not the same as the matter energy density ρ_M in the Einstein equation $\rho_M^H \neq \rho_M$. They are related by the Boltzmann type rate equation of pairs and spacetime, that is studied in this section and shown to be important for understanding the transition between the inflation end and reheating start in next Sec. IV.

A. Particle-antiparticle pair annihilation and decay

We focus on the dynamics and kinematics of particle-antiparticle pairs after they are produced. From the microscopical points of view, the particle-antiparticle pairs can in turn annihilate to the spacetime, i.e., the inverse process of the production process (4)

$$F + \bar{F} \Rightarrow \mathcal{S}. \quad (14)$$

Such back and forth processes

$$\mathcal{S} \Leftrightarrow \bar{F}F, \quad (15)$$

can be regarded as particle-antiparticle emissions and absorptions of the spacetime. As shown in Eqs. (3) and (7), the macroscopic time scale $\tau_H = H^{-1}$ of the spacetime expansion is much longer than the time scale Γ_M^{-1} of microscopic pair productions and annihilations. Therefore, the CPT symmetry of local field theories should be held for microscopic processes, we consider that the

pair-annihilation rate is the same as the pair-production rate

$$\Gamma_M^{\text{Anni}} = \Gamma_M^{\text{Prod}} = \Gamma_M, \quad (16)$$

although the Universe expansion violates the T -symmetry of time translation and reflection.

Henceforth, we introduce the mass parameter \hat{m} to represent not only the effective masses, but also the effective degeneracies of pairs produced in the reheating epoch. That is the substitution $m \rightarrow \hat{m}$ in Eqs. (5,6) and the rate (7) becomes

$$\Gamma_M \approx (\chi \hat{m} / 4\pi) \epsilon. \quad (17)$$

These back and forth processes of massive pairs production and annihilation are due to purely gravitational interactions. Some of massive pairs, however, can also carry the quantum numbers of gauge interactions. Therefore, in addition to their annihilation to the spacetime (14), these “unstable” massive pairs via gauge interactions decay to relativistic particles $\bar{\ell} \ell$, which are much lighter than massive pairs $\bar{F}F$ themselves,

$$\bar{F}F \Rightarrow \bar{\ell} \ell. \quad (18)$$

These relativistic particles $\bar{\ell} \ell$ represent elementary particles in the standard model (SM) of particle physics, and possible massless or massive sterile particles (neutrinos) for the dark matter, for example right-handed neutrinos and composite particles [?] or particles of other theories beyond SM. In general, the decay rate of massive pairs is proportional to the pair mass \hat{m} and can be parametrised as

$$\Gamma_M^{\text{de}} = g_Y^2 \hat{m}, \quad (\bar{F}F \Rightarrow \bar{\ell} \ell) \quad (19)$$

where g_Y is the Yukawa coupling between the massive pairs and relativistic particles.

Taking into account both pair-production and pair-annihilation processes, we study the semi-classical rate equation for the pair energy density ρ_M based on the conservation of the total pair numbers in the Universe evolution obeying Einstein equations (1) and (2).

B. Boltzmann rate equation for particle-antiparticle pairs and spacetime

We adopted the phase space density (the distribution function in phase space) is spatially homogenous and isotropic, and integrating over phase space, we have the pair number density depending only on the time $n_M(t)$, so that the Liouville operator in the phase space for the

kinematic part is just $d(a^3 n_M)/dt = a^3 \dot{n}_M(t) + 3H a^3 n_M(t)$. Adopting the usual approach [12, 37] at the semi-classical level, we use the cosmic rate equation of the Boltzmann type for the pair number density n_M ,

$$\begin{aligned} \frac{dn_M}{dt} + 3H n_M &= \Gamma_M (n_M^H - n_M) - \Gamma_M^{\text{de}} n_M, \\ \frac{d\rho_M}{dt} + 3H \rho_M &= \Gamma_M (\rho_M^H - \rho_M) - \Gamma_M^{\text{de}} \rho_M, \end{aligned} \quad (20)$$

where the second line is due to the massive pairs $\rho_M \approx 2\hat{n}n_M$ and $\rho_M^H \approx 2\hat{n}n_M^H$. These equations effectively describe the pair dynamics of the back and forth processes (15) and decay processes (19) in the Universe evolution. The term $3H n_M$ of the time scale $(3H)^{-1}$ represents the spacetime expanding effect on the the pair density n_M . It should be emphasized that $\Gamma_M n_M^H$ is the source term of pair productions from the space time, and $\Gamma_M n_M$ is the depletion term of pair annihilations into the space time. The spacetime horizon and particle-antiparticle pairs are coupled via the back and forth processes (15). The pair production and annihilation rates are assumed to be equal to Γ_M (16) in the detailed balance term

$$\Gamma_M^{\text{Prod}} n_M^H - \Gamma_M^{\text{Anni}} n_M = \Gamma_M (n_M^H - n_M), \quad (21)$$

in the RHS of the cosmic rate equation (20).

C. A close set of fundamental equations in the reheating epoch

In addition to the cosmic rate equation (20), there is another Boltzmann equation from the conservation of the radiation energy ρ_R of relativistic particles from massive particle decays.

$$\dot{\rho}_R + 4H \rho_R = \Gamma_M^{\text{de}} \rho_M, \quad (22)$$

in the reheating epoch.

As a consequence, we have a close set of four ordinary differential equations to uniquely determine the time evolutions of the Hubble rate H , the cosmological term ρ_Λ , massive pairs' energy density ρ_M and relativistic particles' energy density ρ_R . They are the cosmic rate equation (20) for ρ_M , the reheating equation (22) for ρ_R , Einstein equations (1) and (2) for H and ρ_Λ . In addition, there are three algebraic relations: the pair-production rate Γ_M (17), the pair-decay rate Γ_M^{de} (19) and the spacetime evolution ϵ -rate (3). For further analysis, we recast these equations as the Einstein equations

$$h^2 = \Omega_\Lambda + \Omega_M + \Omega_R, \quad (23)$$

$$\frac{dh^2}{dx} = -3\Omega_M - 4\Omega_R, \quad (24)$$

and the cosmic rate equations

$$\frac{d\Omega_M}{dx} + 3\Omega_M = \frac{\Gamma_M}{H} (\Omega_M^H - \Omega_M) - \frac{\Gamma_M^{\text{de}}}{H} \Omega_M, \quad (25)$$

$$\frac{d\Omega_R}{dx} + 4\Omega_R = \frac{\Gamma_M^{\text{de}}}{H} \Omega_M, \quad (26)$$

where, instead of the cosmic time t , we adopt the cosmic e -folding variable $x = \ln(a/a_{\text{end}})$ and $d(\cdots)/dx = d(\cdots)/(Hdt)$ for the sake of simplicity and significance in physics.

In order to study the reheating epoch, we adopt in Eqs. (23-26) the scale factor a_{end} at the end of the inflation, corresponding the normalisations $h \equiv H/H_{\text{end}}$, $\Omega_{\Lambda, M, R} \equiv \rho_{\Lambda, M, R}/\rho_c^{\text{end}}$ and

$$\Omega_M^H \equiv \frac{\rho_M^H}{\rho_c^{\text{end}}} = \frac{2}{3} \chi \hat{m}^2 h^2, \quad \rho_c^{\text{end}} \equiv \frac{3H_{\text{end}}^2}{(8\pi G)}, \quad (27)$$

in unit of the inflation ending scale H_{end} and the corresponding characteristic density ρ_c^{end} . Using the rates Γ_M (17) and Γ_M^{de} (19), we write the ratios in Eqs. (25) and (26),

$$\frac{\Gamma_M}{H} = \left(\frac{\chi}{4\pi}\right) \left(\frac{\hat{m}}{H_{\text{end}}}\right) \frac{\epsilon}{h}; \quad \frac{\Gamma_M^{\text{de}}}{H} = g_Y^2 \left(\frac{\hat{m}}{H_{\text{end}}}\right) \frac{1}{h}, \quad (28)$$

which represent the rates Γ_M and Γ_M^{de} of the microscopic processes (15) and (19) compared with the Hubble rate H of the macroscopic expansion of the spacetime. Moreover, we rewrite the ϵ -rate (29) of time-varying horizon H as

$$\epsilon \equiv -\frac{1}{H} \frac{dH}{dx} = \frac{3\Omega_M + (4/3)\Omega_R}{2\Omega_\Lambda + \Omega_M + \Omega_R}, \quad (29)$$

to characterise the different episodes of the reheating epoch.

Equations (23-29) can be numerically integrated, provided that the initial conditions (13), see Sec. II C, are given at the beginning of the reheating epoch. This epoch is represented by the scale factor changing from the inflation end $a_3 = a_{\text{end}}$ to the genuine reheating $a_2 = a_R$ in Fig. 1, the schematic diagram of the Universe evolution.

IV. DIFFERENT EPISODES IN THE REHEATING EPOCH

In the reheating epoch, general speaking, the horizon h and the cosmological term Ω_Λ decreases, as the matter content Ω_M or Ω_R increases, meanwhile the ratio Γ_M/H (28) and the ϵ -rate (29) increase. To gain the insight into the physics first, we use the ϵ -rate values (29) to characterize the different episodes in the reheating epoch. In each episode, the ϵ -rate slowly varies in time, we approximately have the time scale of the spacetime expansion

$$H^{-1} \approx \epsilon t. \quad (30)$$

In the transition from one episode to another, the ϵ -rate significantly changes its value. Using the characteristic ϵ values $\epsilon \ll 1, \epsilon \approx 3/2, \epsilon \approx 2$, we identify the following three different episodes \mathcal{P} -*episode*, \mathcal{M} -*episode* and \mathcal{R} -*episode* in the reheating epoch. The \mathcal{P} -*episode* and the \mathcal{M} -*episode* have some similarities to the preheating phase in usual inflation models [2, 3].

A. preheating episode: \mathcal{P} -*episode*

The preheating \mathcal{P} -*episode* is a transition from the inflation end to the reheating start. In this episode, the pair production rate Γ_M (17) is larger than the Hubble rate H , that is still much larger than the pair decay rate Γ_M^{de} (19),

$$\Gamma_M > H \gg \Gamma_M^{\text{de}}, \quad \rho_\Lambda > \rho_M \gg \rho_R. \quad (31)$$

The radiation energy density of relativistic particles is completely negligible $\rho_R \approx 0$, compared with the massive pairs' energy density ρ_M and cosmological one ρ_Λ .

Using the follow values at the inflation end H_{end} (12) and energy density ratio $\rho_M^{\text{end}}/\rho_\Lambda^{\text{end}} \ll 1$ (13), see Sec. IIC,

$$\Omega_M^{\text{end}} = 4.7 \times 10^{-3}, \text{ so that } (\Gamma_M/H)_{\text{end}} \approx 1 \quad (32)$$

as the initial conditions for starting the \mathcal{P} -episode, we numerically integrate Eqs. (23,24) and (25), by selecting values of the mass parameter \hat{m}/m_{pl} .

B. Massive pairs domination: \mathcal{M} -*episode*

After the \mathcal{P} -*episode* transition, the reheating epoch is in the \mathcal{M} -*episode* of massive pair domination. The \mathcal{M} -*episode* is characterised by

$$\rho_M \gg \rho_\Lambda \gg \rho_R, \quad \Gamma_M > H > \Gamma_M^{\text{de}}, \quad (33)$$

so that the radiation energy density ρ_R is negligible in the Einstein equations (1-3) and the cosmic rate equation (20). The H variation ϵ -rate ϵ_M is a constant, shown as an asymptotic value $\epsilon_M \approx 3/2$. In this episode, the Hubble rate H and scale factor $a(t)$ vary as

$$H^{-1} \approx \epsilon_M t, \quad a(t) \sim t^{1/\epsilon_M}, \quad (34)$$

and $h^2 \approx \Omega_M$, the pair energy density $\Omega_M \propto (a/a_{\text{end}})^{-2\epsilon_M}$ drops as in the matter dominated universe, analogously to the scenario [38].

In addition to the large pair energy density ρ_M , the pair production/annihilation rate Γ_M is much larger than the Hubble rate H , i.e., $\Gamma_M/H \gg 1$, see Figure 3 (c) in Ref. [34]. The back and forth processes of pair production and annihilation $\bar{F}F \Leftrightarrow \mathcal{S}$ are important, as described by the cosmic rate equation (25) with the detailed balance term D_M ,

$$D_M \equiv \Gamma_M \left(\Omega_M^H - \Omega_M \right) \quad (35)$$

and the characteristic time scale τ_M ,

$$\tau_M^{-1} \equiv \frac{\Gamma_M}{\Omega_M} \left(\Omega_M^H - \Omega_M \right), \quad (36)$$

which is actually the time period of back and forth $\bar{F}F \Leftrightarrow \mathcal{S}$ oscillating processes. This macroscopic time scale is much smaller than the macroscopic expansion time scale $\tau_H = H^{-1}$, $\tau_M \ll \tau_H$. In this situation, the microscopic back and forth process ($\mathcal{S} \Leftrightarrow \bar{F}F$) is much faster than the horizon expanding process, thus the space time and massive pairs are completely coupled each other via these back and forth processes.

Therefore, the back and forth oscillating process $\bar{F}F \Leftrightarrow \mathcal{S}$ can build a local chemical equilibrium of the quantum-number and energy equipartition

$$\rho_M \Leftrightarrow \rho_M^H; \quad \mu_F + \mu_{\bar{F}} = \mu_{\text{spacetime}} \quad (37)$$

between massive pairs and the space time. The chemical potential of particles is opposite to the chemical potential of antiparticles, i.e., $\mu_F = -\mu_{\bar{F}}$, so that particle and antiparticle pairs have zero chemical potential $\mu_{\text{pair}} = \mu_F + \mu_{\bar{F}} = 0$. The chemical equilibrium (37) leads to the space time “chemical potential” is zero, i.e., $\mu_{\text{spacetime}} = 0$. In this case, the detailed balance term (35) for the oscillations $\rho_M \Leftrightarrow \rho_M^H$ in the microscopic time scale τ_M should vanishes, in the sense of its time-averaged

$$\langle \rho_M - \rho_M^H \rangle = 0, \quad (38)$$

over the macroscopic time $\tau_H \gg \tau_M$. This means that $\rho_M \approx \rho_M^H$ in the macroscopic time scale τ_H . The cosmic rate equation approximately becomes

$$\frac{d\rho_M}{dt} + 3H\rho_M \approx 0, \quad (39)$$

whose solution is $\rho_M \propto a^{-3}$. This is consistent with the solution to Eq. (1) for the massive pair domination $\rho_M \gg \rho_\Lambda$ and $\rho_M \gg \rho_R$, yielding $H^2 \sim \rho_M \propto a^{-3}$. This is also self-consistent with the pair-production formula (5) $\rho_M \approx \rho_M^H = \chi \hat{m}^2 H^2 \propto a^{-3}$.

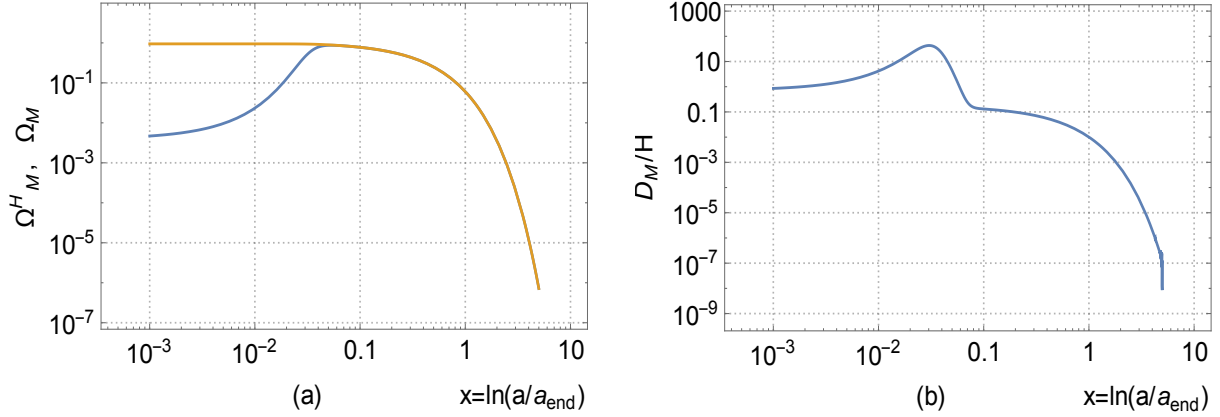


FIG. 2: (Color Online). In a few e -folding number $x = \ln(a/a_{\text{end}})$, (a) the energy density ρ_M^H (27) (orange) of the spacetime produced pairs and the pair energy density of ρ_M (blue) as the solution to the cosmic rate equation (25), showing $\rho_M \approx \rho_M^H$; (b) the detailed balance term D_M (35) vanishes. These illustrations are plotted with the initial condition (32) and parameter $(\hat{m}/m_{\text{pl}}) = 27.7$.

In order to verify these discussions, we check the solution (38) or (39) analytically and numerically. The approximately analytical solution $\rho_M \approx \rho_M^H = \chi \hat{m}^2 H^2$ averaged over the time τ_H consistently obeys the cosmic rate equation (39),

$$\langle \dot{\rho}_M^H \rangle = \langle 2\chi \hat{m}^2 H \dot{H} \rangle = -\langle 2H \rho_M^H \epsilon \rangle \approx -3H \rho_M^H, \quad (40)$$

where $\langle \epsilon \rangle \approx \epsilon_M = 3/2$, and the detailed balance term (35) vanishes. Numerical results quantitatively show the same conclusion: ρ_M approaches to ρ_M^H , and $n_M \approx \rho_M/2\hat{m}$ approaches to $n_M^H \approx \rho_M^H/2\hat{m}$

$$\rho_M \approx \rho_M^H = 2\chi \hat{m}^2 H^2, \quad n_M \approx n_M^H = \chi \hat{m} H^2, \quad (41)$$

see Fig. 2 (a); correspondingly the detailed balance term (35) vanishes, see Fig. 2 (b). The detailed balance solution (41) is valid in the matter dominated evolution, and it is peculiar for stable massive pairs, which have no gauge interactions except gravitation one. In this episode, spacetime and pairs are coupled in horizon H evolution

C. Relativistic particles domination: \mathcal{R} -episode of the genuine reheating

After the \mathcal{M} -episode, the decay term $\Gamma_M^{\text{de}} \Omega_M$ prevails over the detailed balance term D_M (35) in the cosmic rate equation (25), massive pairs undergo the process of decay to relativistic particles, rather than the process of annihilating to the spacetime. The spacetime and pairs are decoupled in

time evolution. It starts the \mathcal{R} -*episode* of the genuine reheating and radiation energy domination, which is characterised by

$$\rho_R \gg \rho_M \gg \rho_\Lambda, \quad \epsilon \rightarrow \epsilon_R \approx 2, \quad (42)$$

and $\Gamma_M^{\text{de}}/H > 1$. As a result, Equations (23) and (24) or Eq. (29) gives

$$H^{-1} \approx \epsilon_R t, \quad a(t)/a_R \approx (t/\tau_R)^{1/\epsilon_R}, \quad (43)$$

where the period of massive particles decay $\tau_R = (\Gamma_M^{\text{de}})^{-1}$ is the reheating time scale and a_R is the scale factor at the genuine reheating. After reheating the matter-energy density is much larger than the cosmological energy density, we show in Ref. [33] due to such back reaction that the cosmological term ρ_Λ tracks down the matter term ρ_M from the reheating end to the radiation-matter equilibrium, then it varies very slowly, $\rho_\Lambda \propto \text{constant}$, consistently leading to the cosmic coincidence in the present time. The detailed discussions and results of such scenario $\tilde{\Lambda}$ CDM have been presented there.

V. PARTICLE AND ANTIPARTICLE OSCILLATING PERTURBATIONS

After a lengthy but necessary preparation, we arrive at the central topic of this article: baryogenesis, magnetogenesis and dark-matter acoustic wave caused by the superhorizon crossings of particle-antiparticle symmetric and asymmetric density perturbations.

We adopt the term ‘‘particle-antiparticle oscillations’’ to stand for the microscopic back and forth processes of the pair production from and annihilation to the spacetime $\mathcal{S} \Leftrightarrow \bar{F}F$. Such particle-antiparticle oscillations have no any preference for particles F or antiparticles \bar{F} , whose numbers are the same in the pair density (5) and the net particle number is exactly zero. On the other hand, this particle and antiparticle symmetry seems to hold true for the local particle-number equipartition or chemical equilibrium $n_M \Leftrightarrow n_M^H$, as the detailed balance term $\Gamma_M (n_M^H - n_M)$ vanishes in the cosmic rate equation (25), as discussed in Sec. IV B. However, these observations are made without carefully considering time scales of the horizon variation and the back and forth processes. In this section, we attempt to present some more detailed analysis on these aspects.

A. Particle density perturbations

Separating particles from antiparticles, we study their density perturbations caused by particle-antiparticle pairs production from and annihilation into the space time, so as to examine symmetric

and asymmetric density perturbations of particles and antiparticles.

1. Continuum and Eulerian equations of particles

Analogously to the study of cosmic perturbation, see for example [12], the linear perturbations of massive particles and antiparticles are separately studied by using their continuum equation and Eulerian equations of Newtonian motion describing two perfect fluids of particle (+) and antiparticle (-) densities $\rho_M^\pm(t, \mathbf{x})$, pressures $p_M^\pm(t, \mathbf{x})$ and velocities $\mathbf{v}_M^\pm(t, \mathbf{x})$ in the Robertson-Walker space time (Freemmann Universe)

$$\dot{\rho}_M^\pm + \nabla \cdot (\rho_M^\pm \mathbf{v}_M^\pm) = -\Gamma_M(\rho_M^\pm - \rho_M^0), \quad (44)$$

$$\dot{\mathbf{v}}_M^\pm + (\mathbf{v}_M^\pm \cdot \nabla) \mathbf{v}_M^\pm = -(\rho_M^\pm)^{-1} \nabla p_M^\pm - \nabla \Phi, \quad (45)$$

$$\nabla^2 \Phi = 4\pi G(\rho_M^+ + \rho_M^-), \quad (46)$$

$$\rho_M^0(t) = (1/2)\rho_M^H = \chi \hat{m}^2 H^2 \quad (47)$$

where the RHS of Eq. (44) contains the source term $\rho_M^0(t)$ and the depletion term ρ_M^\pm . In the last line (47), the unperturbed density $\rho_M^0(t) = \rho_M/2 \approx \rho_M^H/2$ given by Eq. (41). The pair decay term $-\Gamma_M^{\text{de}} \rho_M$ is neglected for the moment. The interacting rate Γ_M and gravitational potential Φ fully respect the symmetry of particle and antiparticle. The arguments in above equations are comoving coordinates (\mathbf{x}, \mathbf{k}) and the time derivative and space gradient are taken with respect to the physical coordinates $(a\mathbf{x}, \mathbf{k}/a)$. The zeroth order solutions ρ_M^\pm to Eqs. (44,45,46) are the density ρ_M^0 of pair productions, which follows the Hubble flow $\mathbf{v}_M^0 = d(a\mathbf{x})/dt = H a \mathbf{x}$, and gives the gravitational potential $\Phi^0 = (2\pi G/3)\rho_M^0 |\mathbf{x}|^2$.

2. Density perturbations of particles and antiparticles

We consider the small perturbations around the averaged values ρ_M^0 and \mathbf{v}_M^0 of massive pairs by writing

$$\delta \mathbf{v}_M^\pm = \mathbf{v}_M^\pm - \mathbf{v}_M^0, \quad \delta \rho_M^\pm = \rho_M^\pm - \rho_M^0 \quad \text{and} \quad \delta_M^\pm = \delta \rho_M^\pm / \rho_M^0. \quad (48)$$

Up to the first order in the perturbative quantities, Equations (44), (45) and (46) become

$$d(\delta \rho_M^\pm)/dt + \rho_M^0 \nabla \cdot (\delta \mathbf{v}_M^\pm) + 3H \delta \rho_M^\pm = -\Gamma_M \delta \rho_M^\pm, \quad (49)$$

$$d(\delta \mathbf{v}_M^\pm)/dt + H \delta \mathbf{v}_M^\pm = -(\rho_M^0)^{-1} \nabla \delta p_M^\pm - \nabla \delta \Phi, \quad (50)$$

and the Poisson equation

$$\nabla^2 \delta\Phi = 4\pi G(\delta\rho_M^+ + \delta\rho_M^-). \quad (51)$$

In terms of $\delta_M^\pm = \delta\rho_M^\pm/\rho_M^0$, Equation (49) yields

$$\nabla \cdot \delta\mathbf{v}_M^\pm = -(\dot{\delta}_M^\pm + \Gamma_M \delta_M^\pm). \quad (52)$$

Taking the gradient of Eq. (50), we arrive at

$$\ddot{\delta}_M^\pm + (\Gamma_M + 2H)\dot{\delta}_M^\pm + (2H\Gamma_M + \dot{\Gamma}_M)\delta_M^\pm = v_s^2 \nabla^2 \delta_M^\pm + 4\pi G\rho_M^0 (\delta_M^+ + \delta_M^-) \quad (53)$$

where the sound velocity

$$v_s = (\delta p_M^\pm / \delta\rho_M^\pm)^{1/2}. \quad (54)$$

Equation (53) represents the perturbations of particle and antiparticle densities caused by the back and forth oscillations of pairs production/annihilation from/to the space time, and it reduces to the usual equation for the density perturbation in the case $\Gamma_M = 0$ and $\dot{\Gamma}_M = 0$.

B. Symmetric and asymmetric density perturbations

Moreover, we introduce the quantity Δ_M to describe the perturbation of the symmetrical particle-antiparticle pair density, and the quantity δ_M to describe the perturbation of the asymmetrical particle-antiparticle density:

$$\Delta_M \equiv (\delta_M^+ + \delta_M^-)/2 = (\rho_M - \rho_M^H)/\rho_M^H, \quad (55)$$

$$\delta_M \equiv (\delta_M^+ - \delta_M^-)/2 = (\rho_M^+ - \rho_M^-)/\rho_M^H. \quad (56)$$

Henceforth, we call Δ_M the pair-density oscillation (perturbation) and δ_M the particle-antiparticle-density oscillation (perturbation). The Δ_M is actually the same as the detailed balance term $(\rho_M - \rho_M^H)$ in the cosmic rate equation (25).

1. Acoustic wave equations for density perturbations

Replacing Eqs. (55) and (56) in Eq. (53), we obtain acoustic wave equations for the density perturbations δ_M and Δ_M ,

$$\ddot{\delta}_M + (\Gamma_M + 2H)\dot{\delta}_M + (2H\Gamma_M + \dot{\Gamma}_M)\delta_M = v_s^2 \nabla^2 \delta_M, \quad (57)$$

$$\ddot{\Delta}_M + (\Gamma_M + 2H)\dot{\Delta}_M + (2H\Gamma_M + \dot{\Gamma}_M)\Delta_M = v_s^2 \nabla^2 \Delta_M + 4\pi G\rho_M^H \Delta_M. \quad (58)$$

It is shown that the modes Δ_M and δ_M satisfy the same type of oscillating equation, except an additional term $4\pi G\rho_M^H \Delta_M$ in Eq. (58) due to the pairs in the external gravitational potential. Because the ϵ -rate (3) varies slowly in the inflation epoch and the \mathcal{M} -episode, we approximately neglect $\dot{\Gamma}_M = (\chi\hat{m}/4\pi)\dot{\epsilon} \gtrsim 0$, except the large ϵ -variation in the transitions: (i) between the inflation end and \mathcal{M} -episode, i.e., \mathcal{P} -episode; (ii) between the \mathcal{M} -episode and \mathcal{R} -episode.

Furthermore, we define the Fourier transformation from $f_M(\mathbf{x}, t) = \Delta_M(\mathbf{x}, t), \delta_M(\mathbf{x}, t)$ to \mathbf{k} modes $f_M^{\mathbf{k}}(t) = \Delta_M^{\mathbf{k}}(t), \delta_M^{\mathbf{k}}(t)$,

$$f_M(\mathbf{x}, t) = \frac{1}{\Omega^{1/2}} \sum_{\mathbf{k}} f_M^{\mathbf{k}}(t) e^{i\mathbf{k}\mathbf{x}}, \quad (59)$$

$$f_M^{\mathbf{k}}(t) = \frac{1}{\Omega^{1/2}} \int d^3x f_M(\mathbf{x}, t) e^{-i\mathbf{k}\mathbf{x}}, \quad (60)$$

where $\Omega = (4\pi/3)H^{-3}$ is the spatial physical volume and $\mathbf{k} = \pi\mathbf{n}/H^{-1}$, $\mathbf{n} = 0, 1, 2, \dots$. The corresponding equations for \mathbf{k} -modes $\delta_M^{\mathbf{k}}$ and $\Delta_M^{\mathbf{k}}$ read,

$$\ddot{\delta}_M^{\mathbf{k}} + (\Gamma_M + 2H)\dot{\delta}_M^{\mathbf{k}} + 2H\Gamma_M\delta_M^{\mathbf{k}} = -(v_s^2|\mathbf{k}|^2/a^2)\delta_M^{\mathbf{k}} \quad (61)$$

$$\ddot{\Delta}_M^{\mathbf{k}} + (\Gamma_M + 2H)\dot{\Delta}_M^{\mathbf{k}} + 2H\Gamma_M\Delta_M^{\mathbf{k}} = -(v_s^2|\mathbf{k}|^2/a^2)\Delta_M^{\mathbf{k}} + 4\pi G\rho_M^H\Delta_M^{\mathbf{k}}. \quad (62)$$

These are semi-classical equations governing the oscillating modes $\delta_M^{\mathbf{k}}$ and $\Delta_M^{\mathbf{k}}$ of frequencies

$$\omega_\delta^2(\mathbf{k}) = 2H\Gamma_M + (v_s^2|\mathbf{k}|^2/a^2) \quad (63)$$

$$\omega_\Delta^2(\mathbf{k}) = 2H\Gamma_M + (v_s^2|\mathbf{k}|^2/a^2) - 4\pi G\rho_M^H. \quad (64)$$

and $(2H\Gamma_M)^{1/2}$ behaves like ‘‘quasi mass’’ term. Due to the oscillations of the pairs-spacetime annihilation and production, the Γ_M -term of pair production and annihilation contributes to the friction coefficient $(\Gamma_M + 2H)$ and oscillation frequency $\omega_{\delta,\Delta}^2(\mathbf{k})$.

Because of the gravitational attraction of pairs produced, the term $4\pi G\rho_M^H$ in Eqs. (62) and (64) could lead to the Jean instability. Observe that in Eq. (64) $4\pi G\rho_M^H = 8\pi\chi(m/M_{\text{pl}})^2H^2$ is much smaller than $2H\Gamma_M + (v_s^2|\mathbf{k}|^2/a^2)$ even for the case $|\mathbf{k}| = 0$ and $m \gg H$ ($v_s^2 \ll 1$) in the inflation and reheating epochs, as well as standard cosmology. Therefore the negative term $4\pi G\rho_M^H$ can be neglected and $\omega_\Delta^2(\mathbf{k}) > 0$, implying the Jeans instability should not occur in these epochs.

2. Oscillating equations of lowest lying modes

We will present and discuss the solutions to these equations (61-64) for the density perturbations in the inflation epoch and three episodes \mathcal{P} , \mathcal{M} and \mathcal{R} of the reheating epoch. We first focus on

the lowest lying oscillation modes by neglecting the pressure term $v_s^2 \nabla^2$ or $(v_s^2 |\mathbf{k}|^2 / a^2)$ terms, since pairs are massive ($m \gg H$) and their sound velocity is small $v_s^2 \ll 1$. Thus, Equations (61-64) become

$$\ddot{\delta}_M^0 + (\Gamma_M + 2H)\dot{\delta}_M^0 + 2H\Gamma_M\delta_M^0 = 0 \quad (65)$$

$$\ddot{\Delta}_M^0 + (\Gamma_M + 2H)\dot{\Delta}_M^0 + 2H\Gamma_M\Delta_M^0 = 0, \quad (66)$$

where the lowest lying oscillation modes $\delta_M^0 \equiv \delta_M^{\mathbf{k}=\mathbf{0}}$ and $\Delta_M^0 \equiv \Delta_M^{\mathbf{k}=\mathbf{0}}$ with the frequencies $\omega_\delta \equiv \omega_\delta(|\mathbf{k}| = \mathbf{0})$ and $\omega_\Delta \equiv \omega_\Delta(|\mathbf{k}| = \mathbf{0})$,

$$\omega_\delta^2 = \omega_\Delta^2 = 2H\Gamma_M. \quad (67)$$

These lowest lying modes are called as the “zero modes” Δ_M^0 and δ_M^0 of pair-density and particle-antiparticle-density oscillations. We stress that in this semi-classical approximation the frequencies (67) of these zero modes weakly depend on the time t in the time period of slowly varying H and Γ_M under consideration. This is different from the usual notion of “mode” with a constant frequency.

To end this section, we would like to mention that the oscillations δ_M^0 are the spacial fluctuations in the number of particles or antiparticles (compositions) per comoving volume, and the oscillations Δ_M^0 are the spacial fluctuations in the number of pairs per comoving volume.

VI. PARTICLE-ANTIPARTICLE ASYMMETRY AND HORIZON CROSSING

In general, it is expected that for large frequencies $\omega_{\delta,\Delta} \gg (\Gamma_M + 2H)$, the modes δ_M^0 and Δ_M^0 are underdamped oscillating inside the horizon. While small frequencies $\omega_{\delta,\Delta} \ll (\Gamma_M + 2H)$, the friction term $(\Gamma_M + 2H)\dot{\delta}_M^0$ dominates, the amplitudes of the modes δ_M^0 and Δ_M^0 are overdamped and frozen to be constants outside the horizon. Following the usual approach, we present a quantitative analysis to show this phenomenon by using the simplified Eqs. (65,66) and (67) in one dimension and assuming isotropic tree-dimension oscillations.

A. Under- and over-damped oscillating modes and horizon crossing

In terms of dimensionless variables $t \rightarrow \hat{m}t$, $\Gamma_M \rightarrow \Gamma_M/\hat{m}$ and $H \rightarrow H/\hat{m}$, we rewrite Eq. (65) in the form of the usual equation for a spherical harmonic oscillator in three dimension,

$$\ddot{\delta}_M^0 + 2\zeta\omega_\delta\dot{\delta}_M^0 + \omega_\delta^2\delta_M^0 = 0, \quad (68)$$

and the same for the mode Δ_M^0 . The underdamped frequency ω_δ and the damping ratio ζ are,

$$\omega_\delta^2 \equiv 2\Gamma_M H, \quad \zeta \equiv (\Gamma_M + 2H)/(2\omega_\delta), \quad (69)$$

which depends on time, because the spacetime expanding rate $H(t)$ and the pair production/annihilation rate $\Gamma_M(t)$ vary in time.

1. Under- and over-damped oscillating modes

We further assume the slowly time-varying ω_δ and ζ , roughly treated as constants, compared with the rapidly time-varying modes Δ_M^0 and δ_M^0 under considerations. In this circumstance, the approximate solution to Eq. (68) reads

$$\delta_M^0 \propto e^{-\omega_\delta \zeta t} e^{-i\omega_\delta(1-\zeta^2)^{1/2}t}. \quad (70)$$

We have following physical situations:

- (i) in the underdamped case ($\zeta < 1$), i.e., $2\omega_\delta > \Gamma_M + 2H$, the modes δ_M^0 and Δ_M^0 oscillate with smaller frequencies than ω_δ , their wavelengths are smaller than the horizon size, and amplitudes damped to zero inside the horizon. The damping time scale $(\omega_\delta \zeta)^{-1} = (\Gamma_M + H)^{-1} \approx \Gamma_M^{-1}$;
- (ii) in the overdamped case ($\zeta > 1$), i.e., $2\omega_\delta < \Gamma_M + 2H$, the modes δ_M^0 and Δ_M^0 's wavelengths are larger than the horizon size, their amplitudes exponentially decay and return to steady states without oscillating. In the case ($\zeta \gg 1$), the solution (70) yields $\delta_M^0, \Delta_M^0 \propto \text{const.}$, indicating the amplitudes of modes δ_M^0 and Δ_M^0 are “frozen” to constants outside the horizon.

2. Lowest lying mode crossing horizon

The separatrix between the situations (i) and (ii) is defined at $\zeta = 1$. At this separatrix, the definitions (69) of the frequency ω_δ and damping ratio ζ lead to

$$\Gamma_M = 2H, \quad (71)$$

and the critical ratio of horizon radius and pair oscillating wavelength

$$\frac{H^{-1}}{\omega_\delta^{-1}} = \left(\frac{2\Gamma_M}{H} \right)^{1/2} = 2. \quad (72)$$

Such a critical ratio (72) represents the horizon crossing of the zero modes δ_M^0 and Δ_M^0 :

- (a) the δ_M^0 and Δ_M^0 modes are *inside* the horizon for $(H^{-1}/\omega_\delta^{-1}) = (2\Gamma_M/H)^{1/2} > 2$;
- (b) the δ_M^0 and Δ_M^0 modes are *outside* the horizon for $(H^{-1}/\omega_\delta^{-1}) = (2\Gamma_M/H)^{1/2} < 2$.

These results have clear physical meanings. Whether the oscillating modes is subhorizon size or superhorizon size crucially depends on the “time-competition” (71) between the rate Γ_M of the back and forth oscillating process $\mathcal{S} \Leftrightarrow \bar{F}F$ and the Hubble rate H of spacetime expansion: $\Gamma_M > H$ the modes stay inside the horizon; $\Gamma_M < H$ the modes stay outside the horizon. In other words, the modes stay inside (outside) the horizon, if they oscillate faster (slower) than the spacetime expanding rate, since they have (no) enough time to keep themselves inside the horizon. Consistently, the “space-competition” (72) of horizon size and mode wavelength shows (a) subhorizon sized modes and (b) superhorizon sized modes.

The horizon crossing condition (72) clearly depends on the functions $H(t)$ and $\Gamma_M(t)$ in different epochs of the Universe evolution. Using the pair-production rate expression Γ_M (17) at the horizon crossing, we find the horizon crossing condition (71) for the zero mode to be

$$H_{\text{cr}} = \Gamma_M^{\text{cr}}/2, \quad \Gamma_M^{\text{cr}} = \chi \hat{m} \epsilon_{\text{cr}} / (4\pi), \quad (H_{\text{cr}}/\hat{m}) = (\chi/8\pi) \epsilon_{\text{cr}}, \quad (73)$$

where H_{cr} and ϵ_{cr} stand for the Hubble scale and ϵ -rate at the horizon crossing. The LHS is the ratio of particle Compton length and horizon radius, the RHS is the ϵ -rate (29) depending on dynamical evolution, and $\chi = 1.85 \times 10^{-3}$ characterizes the width $1/(\chi \hat{m})$ on the horizon surface where massive pairs are produced.

We end this section by noting that the term $\dot{\Gamma}_M \propto \dot{\epsilon} > 0$ in Eqs. (57) and (58) might not be negligible for time-increasing ϵ -rate in the \mathcal{P} -episode. However, the effective oscillating frequencies $\omega_\delta = 2H\Gamma_M + \dot{\Gamma}_M > 2H\Gamma_M$ (wavelengths ω_δ^{-1}) become larger (smaller), so that the critical ratio (72) should be larger than 2.

B. Symmetric and asymmetric oscillating amplitudes at horizon crossing

To quantify symmetric and asymmetric oscillating amplitudes at horizon crossing, the root-mean-square (*rms*) density fluctuations are defined by

$$\bar{\delta}_M \equiv \langle \delta_M(\mathbf{x}) \delta_M^\dagger(\mathbf{x}) \rangle^{1/2}, \quad \bar{\Delta}_M \equiv \langle \Delta_M(\mathbf{x}) \Delta_M^\dagger(\mathbf{x}) \rangle^{1/2} \quad (74)$$

where $\langle \dots \rangle = \Omega^{-1} \int d^3x (\dots)$ indicates the average all states over the space. The use of Fourier transformations (59) and (60) yields

$$\bar{\delta}_M^2 = \frac{1}{\Omega} \sum_{\mathbf{k}, \mathbf{k}'} \delta_M^{\mathbf{k}} \delta_M^{\mathbf{k}'\dagger} \delta_{\mathbf{k}, \mathbf{k}'} = \frac{1}{\Omega} \sum_{\mathbf{k}} |\delta_M^{\mathbf{k}}|^2 \quad (75)$$

and the same for $\bar{\Delta}_M^2$, where the dimensionless $\delta_{\mathbf{k},\mathbf{k}'} = \Omega^{-1} \int d^3x e^{i\mathbf{x}\cdot(\mathbf{k}-\mathbf{k}'')}$ is the Kronecker delta function of discrete variables \mathbf{k} and \mathbf{k}' .

1. Lowest lying mode amplitudes at horizon crossing

Considering only contribution from the lowest lying modes of underdamped oscillating δ_M^0 and Δ_M^0 , from Eq. (75) we approximately obtain

$$\bar{\delta}_M^2 \approx \Omega^{-1} |\delta_M^0|^2, \quad \bar{\Delta}_M^2 \approx \Omega^{-1} |\Delta_M^0|^2. \quad (76)$$

At a fixed time t , the amplitudes $|\delta_M^0|^2$ and $|\Delta_M^0|^2$ of the lowest lying state (ground state) of underdamped harmonic oscillator (68) can be expressed by the characteristic length scale $1/(2m\omega_\delta)^{1/2}$ of the oscillation,

$$|\delta_M^0|^2 \approx 1/(2\hat{m}\omega_\delta)^{3/2}, \quad |\Delta_M^0|^2 \approx 1/(2\hat{m}\omega_\Delta)^{3/2}, \quad (77)$$

see, e.g., Refs. [40], [41], and [39]. If the wavelength of the lowest lying state is much smaller than the horizon radius, the ground state will evolve adiabatically, and Eq. (77) will continue to hold at later times, thus we obtain the root-mean-square of density fluctuations (74)

$$\bar{\delta}_M^2 = \bar{\Delta}_M^2 \approx \frac{1}{4\pi(2\hat{m})^{3/2}} \frac{3H^3}{(2H\Gamma_M)^{3/2}}. \quad (78)$$

At the other extreme, if the wavelength of the lowest lying state is much larger than the horizon radius, the oscillator will be overdamped, and the oscillating amplitudes $\bar{\delta}_M$ and $\bar{\Delta}_M$ will remain constants with time. These constants at the horizon crossing $H_{\text{cr}} = \Gamma_M^{\text{cr}}/2$ (73) are

$$\bar{\delta}_M = \bar{\Delta}_M \approx \left(\frac{3}{32\pi}\right)^{1/2} \left(\frac{H_{\text{cr}}}{\hat{m}}\right)^{3/4} = \left(\frac{3}{32\pi}\right)^{1/2} \left(\frac{\chi\epsilon_{\text{cr}}}{8\pi}\right)^{3/4}, \quad (79)$$

whose values depend on the Hubble rate H or the ϵ -rate at the horizon crossing.

2. Particle-antiparticle asymmetry due to horizon crossing

As a result, using Eqs. (55) and (56), we explicitly write the result (79) as,

$$\rho_M^+ - \rho_M^- = \bar{\delta}_M \rho_M^H, \quad (80)$$

$$\rho_M - \rho_M^H = \bar{\Delta}_M \rho_M^H, \quad (81)$$

where the right-handed sides are in the sense of *rms*. In other words, $\bar{\delta}_M \rho_M^H$ represents the spacial fluctuations in the number of particles or antiparticles (compositions) per comoving volume, and

$\bar{\Delta}_M \rho_M^H$ represents the spacial fluctuations in the number of pairs per comoving volume. This result physically implies the following two consequences due to the particle-antiparticle oscillations at the horizon crossing:

- (i) In the case that the δ_M is an underdamped oscillating mode inside the horizon, its root-mean-squared (*rms*) value $\bar{\delta}_M$ vanishes, indicating all particles and antiparticles are inside the horizon, no net particle number appears with respect to the observer inside the horizon. The particle-antiparticle symmetry holds.
- (ii) In the case that the δ_M is an overdamped oscillating mode frozen outside the horizon, its root-mean-squared (*rms*) value $\bar{\delta}_M$ does not vanish, indicating some particles (or anti-particles) are outside the horizon, thus net particle number appears with respect to the observer inside the horizon. The particle-antiparticle symmetry breaks. The “frozen” amplitudes of $\bar{\delta}_M$ and $\bar{\Delta}_M$ are very small $\sim \mathcal{O}[(H/m)^{3/4}]$ (79) on the horizon surface, where the production and annihilation of particle and anti-particles take place.

It is important to note that the total number of particles and antiparticles inside and outside the horizon is preserved. In the second case (ii), the positive (negative) net number of particles and antiparticles viewed by a subhorizon observer has to be equal to the negative (positive) net number of particles and antiparticles outside the horizon, which is described by the asymmetric perturbation $\bar{\delta}_M$ on the surface of the horizon crossing.

VII. HORIZON CROSSINGS AT REHEATING START AND END

As discussed in the previous section, the lowest lying mode δ_M inside the horizon represents an underdamping oscillation between particles and antiparticles and its dampened amplitude vanishes within the horizon. As a result, the averaged net number of particles is zero in this time period $t \sim H^{-1}$, and the symmetry of particle and antiparticle is preserved. Instead, the lowest lying mode δ_M outside the horizon means that its amplitude is frozen to a constant $\delta_M = \text{const.} \neq 0$. This implies that the observer inside the horizon should observe a non-vanishing net particle number associating the horizon surface, representing the modes of constant amplitude outside the horizon. Such mode horizon crossing indicates the asymmetry of particle and antiparticle occurs. Now we need to examine where such mode horizon crossing takes place in the early Universe evolution. The same discussions apply to the mode Δ_M (55) describing the perturbations of the pair density, which however do not violate the symmetry of particle and antiparticle.

A. Subhorizon crossing in preheating \mathcal{P} -episode

In order to find the subhorizon crossing in preheating \mathcal{P} -episode, we first examine that the modes δ_M and Δ_M are superhorizon size in the pre-inflation and inflation epoch, while they are subhorizon size in the massive pair oscillating \mathcal{M} -episode.

1. Particle-antiparticle asymmetry in pre-inflation and inflation

In the pre-inflation and inflation epoch $H > \Gamma_M$, the modes δ_M and Δ_M are outside the horizon, corresponding to the overdamped case ($\zeta > 1$). This can be also seen by the ratio of horizon radius H^{-1} and pair oscillating wave length ω_δ^{-1} (67),

$$\frac{H^{-1}}{\omega_\delta^{-1}} = \left(\frac{H^{-2}}{2^{-1}\Gamma_M^{-1}H^{-1}} \right)^{1/2} < \left(\frac{\Gamma_M^{-1}}{2^{-1}\Gamma_M^{-1}} \right)^{1/2} = 2^{1/2}, \quad (82)$$

indicating $H^{-1}/\omega_\delta^{-1} < 2$. This is numerically shown in Fig. 3 (a), where the blue line $H^{-1}/\omega_\delta^{-1}$ is below the orange line 2. This implies that in the inflation, the modes δ_M and Δ_M wavelengths are larger than the horizon size, their amplitudes exponentially decay and return to steady states without oscillating, indicating that the modes δ_M and Δ_M are superhorizon size, and their amplitudes of modes δ_M and Δ_M are “frozen” to constants outside the horizon. With respect to an observer inside the horizon, this means that with respect to an observer inside the horizon, $\bar{\delta}_M$ (80) does not vanish ($\bar{\delta}_M \neq 0$) and the particle-antiparticle asymmetry holds in the pre-inflation ($a < a_4$) and inflation epoch ($a_4 < a < a_3$), as indicated in Fig. 1.

2. Particle-antiparticle symmetry in \mathcal{M} -episode

In the \mathcal{M} -episode $H < \Gamma_M/2$, however, we find that the modes δ_M and Δ_M are inside the horizon. This is because the ratio of horizon radius and pair oscillating wavelength is larger than 2,

$$\frac{H^{-1}}{\omega_\delta^{-1}} = \left(\frac{H^{-2}}{2^{-1}H^{-1}\Gamma_M^{-1}} \right)^{1/2} > \left(\frac{2\Gamma_M^{-1}}{2^{-1}\Gamma_M^{-1}} \right)^{1/2} = 2, \quad (83)$$

indicating that the modes δ_M and Δ_M are subhorizon sized underdamped oscillations, corresponding to the underdamped case ($\zeta < 1$). This is numerically shown in Fig. 3 (a), where the blue line $H^{-1}/\omega_\delta^{-1}$ is above the orange line 2. Therefore, in the \mathcal{M} -episode the particle-antiparticle asymmetric mode δ_M and symmetric mode Δ_M are well inside the horizon, behaving as underdamped oscillating waves whose dampened amplitudes vanish within the horizon H^{-1} . Their

root-mean-square density fluctuations (74) $\bar{\delta}_M = 0$ and $\bar{\Delta}_M = 0$ vanish, as discussed using density perturbations in previous section. This means that with respect to an observer inside the horizon, the asymmetric perturbation $\bar{\delta}_M$ (80) vanishes ($\bar{\delta}_M = 0$) and the particle-antiparticle symmetry holds in the \mathcal{M} -episode, $a_3 < a < a_2$, as indicated in the sketch of Fig. 1.

This physical situation can be also understood using the cosmic rate equation (25) discussed in Sec. III B. The $\bar{\delta}_M = 0$ and $\bar{\Delta}_M = 0$ equivalently correspond to the averaged $\langle \delta_M \rangle = 0$ and $\langle \Delta_M \rangle = 0$ over the time period $H^{-1} \sim t > \tau_M$ larger than the characteristic oscillating time scale τ_M (36). In fact, the $\langle \Delta_M \rangle = 0$ corresponds to the detailed balance $\rho_M \Leftrightarrow \rho_M^H = 2\chi\hat{m}^2 H^2$ in the cosmic rate equation (25), see discussions in Sec. IV B. This implies that the detailed balance between the pair productions and annihilations inside the horizon, therefore the net number of particles and antiparticles is zero and the particle-antiparticle symmetry is preserved.

3. Subhorizon crossing and particle-antiparticle symmetry

Form the superhorizon size (82) in the inflation epoch to the subhorizon size (83) in the \mathcal{M} -episode, the modes δ_M and Δ_M cross at least once the horizon. Because the H and Γ_M vary monotonically, Equations (82) and (83) show that one horizon crossing point $\omega_\delta = H$ locates at $H = \Gamma_M/2$ in the preheating \mathcal{P} -episode. Using Eq. (71), we find the subhorizon crossing scale H_{crin} and the oscillating frequency $\omega_\delta^{\text{crin}}$ at the crossing scale factor a_{crin} ,

$$H_{\text{crin}} = \Gamma_M/2 = H_{\text{end}}/2, \quad \omega_\delta^{\text{crin}} = (2\Gamma_M H)^{1/2} = H_{\text{end}}, \quad (84)$$

which are the same order of the inflation end scale H_{end} (12). In Fig. 3 (a), using numerical results we plot the ratio $H^{-1}/\omega_\delta^{-1} = (2\Gamma_M/H)^{1/2}$ (83), starting from the inflation end $H = \Gamma_M$, to show the subhorizon crossing takes place at $x = \ln(a_{\text{crin}}/a_{\text{end}}) \approx 5 \times 10^{-3}$, i.e., $a_{\text{crin}} \approx 1.01a_{\text{end}}$ in the preheating \mathcal{P} -episode. This shows that the subhorizon crossing occurs right after the inflation end, the scale factor $a_{\text{crin}} \gtrsim a_{\text{end}}$, i.e., a_3 indicated in the sketch of Fig. 1.

In the pre-inflation and inflation epoch, the subhorizon observer views the particle-antiparticle asymmetry because some of particles or antiparticles are outside the horizon. When these superhorizon particles or antiparticles cross back the horizon, the subhorizon observer views all particles and antiparticles, therefore the particle-antiparticle symmetry. The amount of particles or antiparticles subhorizon crossing at a_{crin} can be calculated as follow. The numerical value $\epsilon_{\text{cr}} = \epsilon_{\text{crin}} \approx 1.0 \times 10^{-2}$ at the subhorizon crossing a_{crin} can be found from the Figure 6 (c) of Ref. [34] and we use Eq. (79) to calculate the asymmetric and symmetric pair density perturba-

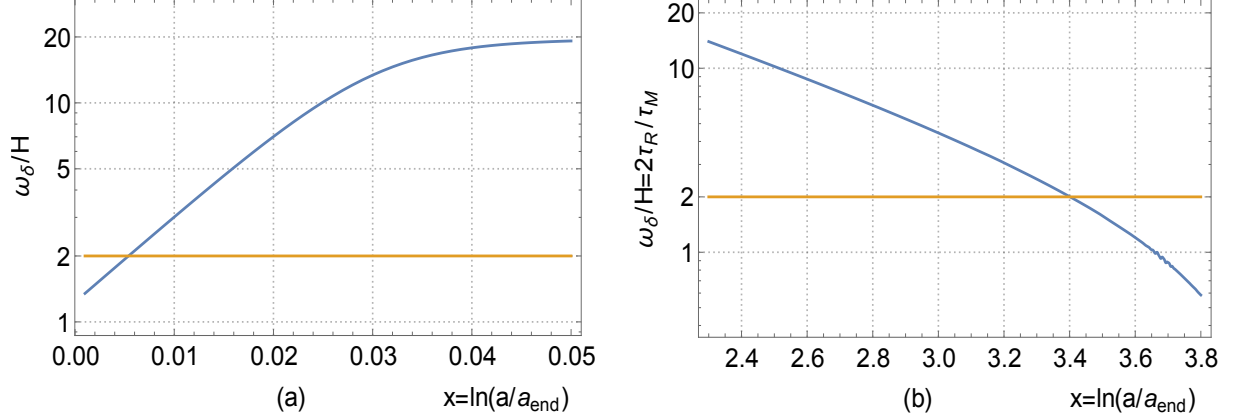


FIG. 3: (Color Online). In terms of the e -folding number $x = \ln(a/a_{\text{end}})$, the ratio of the horizon size H^{-1} and the oscillating wave length ω_δ^{-1} , i.e., $H^{-1}/\omega_\delta^{-1} = \omega_\delta/H$ (83) is plotted (blue) compared with the horizon crossing $\omega_\delta/H = 2$ (orange). Superhorizon (subhorizon) is below (above) the orange horizontal line. (a) The ratio $\omega_\delta/H = (2\Gamma_M/H)^{1/2}$ (72) (blue) in the preheating \mathcal{P} -episode. The modes (blue line) evolve in the scale factor a from superhorizon size to subhorizon size. (b) The ratio $\omega_\delta/H \approx (2\tau_R/\tau_M)$ (88) (blue) in the genuine reheating \mathcal{R} -episode. The modes (blue line) evolve in the scale factor a from subhorizon size to superhorizon size. In these two figures (a) and (b), the parameters $\hat{m}/m_{\text{pl}} = 27.7$ and $g_Y^2 = 10^{-9}$.

tions

$$\bar{\delta}_M^{\text{crin}} = \bar{\Delta}_M^{\text{crin}} \approx 4.33 \times 10^{-6}, \quad (85)$$

at the subhorizon crossing. Then the net particle density perturbation (80) and the pair density perturbation (81) at the horizon crossing (84) are given by,

$$\rho_M^+ - \rho_M^- = \bar{\delta}_M^{\text{crin}} \rho_M^H \approx \bar{\delta}_M^{\text{crin}} (\hat{m}^2 H_{\text{end}}^2)/2, \quad (86)$$

$$\rho_M - \rho_M^H = \bar{\Delta}_M^{\text{crin}} \rho_M^H \approx \bar{\Delta}_M^{\text{crin}} (\hat{m}^2 H_{\text{end}}^2)/2. \quad (87)$$

They are about 10^{-3} in unit of the characteristic density $\rho_{\text{end}}^c = 3m_{\text{pl}}H_{\text{end}}^2$ (27) in the preheating \mathcal{P} -episode. The partice-antiparticle asymmetry (86) is on the horizon surface at the subhorizon crossing. It represents the superhorizon partice-antiparticle asymmetry in the pre-inflation and inflation epochs. It also represents the subhorizon restoration of the partice-antiparticle symmetry in the massive pair oscillating \mathcal{M} -episode.

After the subhorizon crossing (84), the subhorizon sized modes δ_M and Δ_M remain inside the horizon as underdamped oscillating modes in the massive pair oscillating \mathcal{M} -episode, as shown in Fig. 3 (a), until they undergo the superhorizon crossing again.

B. Superhorizon crossing in genuine reheating \mathcal{R} -episode

We are going to show the modes δ_M and Δ_M superhorizon crossing in the transition from the massive pair oscillating \mathcal{M} -episode to the genuine reheating \mathcal{R} -episode, when massive pairs predominately decay into relativistic particles.

1. Superhorizon crossing in genuine reheating \mathcal{R} -episode

In the genuine reheating \mathcal{R} -episode, the horizon scale H is mainly determined by the pair decay rate Γ_M^{de} , since the pair decay rate Γ_M^{de} (time τ_R) is much larger (shorter) than that of the pair oscillations. In order to see the whether modes δ_M and Δ_M are subhorizon size or superhorizon size in the \mathcal{R} -episode, we use the criteria (71) or (72),

$$\frac{H^{-1}}{\omega_\delta^{-1}} = \left(\frac{2\Gamma_M}{H}\right)^{1/2} \approx 2(\tau_R\Gamma_M)^{1/2} = 2\left(\frac{\Gamma_M}{\Gamma_M^{\text{de}}}\right)^{1/2} < 2, \quad (88)$$

where $\tau_R^{-1} = \Gamma_M^{\text{de}}$, we adopt the horizon size H^{-1} approximately determined by the reheating scale H_{RH} at the scale factor a_R , see Eq. (73) of Ref. [34] or the first equation in (5.74) of Ref. [12],

$$H_{\text{RH}}^2 = (2\tau_R)^{-2} = (\Gamma_M^{\text{de}}/2)^2, \quad (89)$$

and $\Gamma_M^{\text{de}} > \Gamma_M$ in the \mathcal{R} -episode. The inequality (88) or $\Gamma_M < 2H_{\text{RH}} \approx \Gamma_M^{\text{de}}$ [see Eq. (71)] shows that the modes δ_M and Δ_M are superhorizon sizes in the \mathcal{R} -episode. Therefore, from the subhorizon sized modes δ_M and Δ_M in the \mathcal{M} -episode to the superhorizon sized modes δ_M and Δ_M in the \mathcal{R} -episode, the superhorizon crossing must take place in the transition between the \mathcal{M} -episode and the \mathcal{R} -episode. The superhorizon crossing occurs at $H^{-1}/\omega_\delta^{-1} = 2$, yielding

$$H_{\text{crou}} = \Gamma_M^{\text{crou}}/2 \approx \Gamma_M^{\text{de}}/2, \quad \Gamma_M^{\text{crou}} \approx \Gamma_M^{\text{de}}, \quad (90)$$

consistently with the horizon crossing condition (71) or (72). The approximation $\Gamma_M^{\text{crou}} \approx \Gamma_M^{\text{de}}$ comes from $H_{\text{crou}} \approx H_{\text{RH}} = (\Gamma_M^{\text{de}}/2)$. This implies that the superhorizon crossing occurs at the scale factor scale a_{crou} close to a_R of the genuine reheating, and the corresponding scale H_{crou} close to the reheating scale H_{RH}

$$H_{\text{crou}} \gtrsim H_{\text{RH}}, \quad a_{\text{crou}} \lesssim a_R, \quad (91)$$

as indicated by the scale factor $a_{\text{crou}} \lesssim a_R = a_2$ in the sketch of Fig. 1.

In order to verify such superhorizon crossing point (90), we perform the numerical calculations by using the close set of fundamental equations (23-26) and relations (27-29). In this case, both

the decay term $\Gamma_M^{\text{de}}\Omega_M$ and the oscillating term $\Gamma_M(\Omega_M^H - \Omega_M)$ in the cosmic rate equation (25) are important and comparable. The former is described by the time scale τ_R (43) and the latter by the time scales τ_M (36). The pair oscillating frequency $\omega_{\delta,\Delta}$ is actually characterised by the time scale τ_M , namely $\omega_\delta = \omega_\Delta \approx \tau_M^{-1}$. We numerically compute the ratio $H^{-1}/\omega_\delta^{-1} \approx 2\tau_R/\tau_M$ of the horizon radius and pair oscillating wavelength, and plot it (blue line) against 2 (orange line) in Fig. 3 (b). It shows that the ratio $H^{-1}/\omega_\delta^{-1}$ (blue line) varies from > 2 to < 2 , showing the superhorizon crossing in the genuine reheating \mathcal{R} -episode. From Fig. 3 (b), it is found that the superhorizon crossing $H_{\text{crou}}t$ and $a_{\text{crou}}t$ (91) are indeed close to the genuine reheating H_{RH} and a_R (89), approximately equal to the one determined by $\tau_R \approx \tau_M$ in the Figure 7 (c) and (d) of Ref. [34].

2. Initial particle-antiparticle asymmetry for standard cosmology

As illustrated in Figs. 3 (a) and (b), the modes δ_M and Δ_M have the subhorizon crossing (84) in the preheating \mathcal{P} -episode and superhorizon crossing (91) in the genuine reheating \mathcal{R} -episode. The subhorizon observer views:

- (i) the particle and antiparticle asymmetry in the pre-inflation and inflation epochs before the subhorizon crossing (84), and the asymmetry is calculated in Eq. (86);
- (ii) the particle and antiparticle symmetry in the massive pair oscillating \mathcal{M} -episode in between the preheating and the genuine reheating;
- (iii) the particle and antiparticle asymmetry in the standard cosmology epoch after the genuine reheating \mathcal{R} -episode.

The cases (i) and (ii) have been discussed. We focus the discussions on the case (iii) and calculate the particle and antiparticle asymmetry, relating to the net number of particles viewed by the subhorizon observer in the standard cosmology epoch.

Due to the superhorizon crossing $a_{\text{crou}}t \lesssim a_R$, the δ_M is an overdamped oscillating mode frozen outside the horizon, its root-mean-squared (*rms*) value $\bar{\delta}_M$ does not vanish, indicating some particles (or anti-particles) are outside the horizon, thus net particle number appears with respect to the subhorizon observer in the standard cosmology epoch, as indicated $a > a_2 = a_R \gtrsim a_{\text{crou}}t$ in the sketch of Fig. 1.

Using Eq. (79), we calculate the asymmetric and symmetric pair density perturbations at the superhorizon crossing (90).

$$\bar{\delta}_M^{\text{crou}} = \bar{\Delta}_M^{\text{crou}} = 2.31 \times 10^{-4}, \quad (92)$$

where the ϵ -rate value $\epsilon_{\text{cr}} = \epsilon_{\text{crou}} \lesssim 2$ closes to the genuine reheating \mathcal{R} -episode.

Based on Eq. (80), we calculate the particle-antiparticle asymmetric number density, i.e., the net number density of particles and antiparticles,

$$\delta n_M^{\text{crou}} = \frac{\rho_M^+ - \rho_M^-}{2\hat{m}} = \bar{\delta}_M^{\text{crou}} n_M^H, \quad (93)$$

where $n_M^H \approx \rho_M^H / (2\hat{m}) \approx \chi \hat{m} H_{\text{crou}}^2$ at the superhorizon crossing a_{crou} . As a result, we approximately obtain the net number density of massive particles and antiparticles,

$$\delta n_M^{\text{crou}} = \frac{\rho_M^+ - \rho_M^-}{2\hat{m}} \Big|_{\text{crou}} \approx 2.31 \times 10^{-4} n_M^H \Big|_{\text{crou}}, \quad (94)$$

here the subscript ‘‘crou’’ refers to the horizon crossing (91), and

$$n_M^H \Big|_{\text{crou}} \approx \rho_M^H / (2\hat{m}) \Big|_{\text{crou}} \approx \chi \hat{m} H_{\text{RH}}^2. \quad (95)$$

Analogously from Eq. (81), we obtain the pair number density perturbation of massive particles,

$$\Delta n_M^{\text{crou}} = \frac{\rho_M - \rho_M^H}{2\hat{m}} \Big|_{\text{crou}} \approx 2.31 \times 10^{-4} n_M^H \Big|_{\text{crou}}. \quad (96)$$

This net number density (94) of massive particles and antiparticles is the initial value of the asymmetric (net) numbers of particles and antiparticles in the standard cosmology.

Such a nonzero net number of particles and antiparticles inside the horizon is preserved in the entire history of the standard cosmology, because there is no another subhorizon crossing of the asymmetric mode δ_M after the superhorizon crossing (91). The reasons are the following. As the horizon scale H decreases, the spacetime produced pairs have a small density $\rho_M^H = 2\chi m^2 H^2$ and the horizon H evolution is governed by the matter produced in the reheating. They rapidly decay to relativistic particles for $\tau_R \ll \tau_M$, and the oscillation $\mathcal{S} \Leftrightarrow \bar{F}F$ is no longer relevant. Therefore, the superhorizon condition $H^{-1}/\omega_\delta < 2$ (88) holds. The asymmetric modes δ_M carried the net particle number have been frozen in the superhorizon, and not reentered back to the horizon again.

It is important to note that the total number of particles and antiparticles inside and outside the horizon is zero and preserved. The positive (negative) net number of particles and antiparticles viewed by a subhorizon observer has to be equal to the negative (positive) net number of particles and antiparticles outside the horizon, which is described by the asymmetric perturbation $\bar{\delta}_M$ on

the surface of the superhorizon crossing. The sum of these two net numbers is identically zero, because the particle and antiparticle symmetry is preserved in the $\mathcal{S} \Leftrightarrow \bar{F}F$ processes, pair decay process $\bar{F}F \Rightarrow \bar{\ell} \ell$ and all other microscopic processes respect the CPT symmetry.

VIII. BARYOGENESIS AND MAGNETOGENESIS IN REHEATING EPOCH

A tiny asymmetry (net number) of particles and antiparticles remains inside the horizon and the subhorizon observer sees a nonzero net number of particles and antiparticles that is preserved in the entire history of the standard cosmology. We will show that the asymmetry of massive particles F and antiparticles \bar{F} results in the asymmetry of baryon numbers of baryons B and antibaryons \bar{B} in the Universe, and the net number density (94) leads to the baryogenesis in agreement with observations.

A. Origin of net baryon numbers

Following the way discussed in Ref. [12], using the net particle number density $\delta n_M^{\text{crou}}t$ (94), and the continuum equation of the net baryon number density n_B , we obtain

$$\begin{aligned} \dot{n}_B + 3Hn_B &= \delta n_M^{\text{crou}}t / \tau_R, \\ \Rightarrow n_B(a) &= 2.31 \times 10^{-4} n_M^H(a_R) \left(\frac{a}{a_R} \right)^{-3} [1 - \exp -t/\tau_R]. \end{aligned} \quad (97)$$

In the second line of integration, the initial moment $t_i \ll \tau_R$ is assumed and the solution for massive pairs ρ_M decay is used, see Eq. (66) of Ref. [34] or the first equation in (6.61) of Ref. [12]. The physical content is clear: at the late times, $t \gg \tau_R$, the net baryon number per comoving volume $a^3 n_B(a)$ is just 2.31×10^{-4} times the initial number of massive particle F 's per comoving volume $a_R^3 n_M^H(a_R)$. Note that $a^3 n_B(a)$ the comoving number density, whereas $n_B(a)$ is the physical number density, i.e., the net baryon number per physical volume. Since the decay time scale $\tau_R \propto \hat{m}^{-1}$ is very short, we adopt the approximation that the horizon crossing coincides with the genuine reheating (91) ($a = a_R \approx a_{\text{crou}}t$ and $t \approx \tau_R$) to obtain the net baryon number density

$$n_B^R(a_R) = 1.46 \times 10^{-4} n_M^H(a_R), \quad n_M^H(a_R) = \chi \hat{m} H_{\text{RH}}^2, \quad (98)$$

yielding the origin of the net number of baryons or antibaryons, i.e., the baryogenesis in the Universe.

As an asymmetric relic from the reheating epoch or an initial asymmetric state of the standard cosmology, the net baryon number (98) remains inside the horizon and conserves in subsequent

Universe evolutions, accounting for the baryon and anti-baryon asymmetry observed today. It should be emphasised that in our scenario the standard cosmology starts from the initial state of asymmetrical baryon and antibaryon numbers, so that the three Sakharov criterion [42] for the baryogenesis are not applicable.

B. Baryon number-to-entropy ratio

Using the entropy S_R and temperature T_{RH} of the reheating epoch, obtained in Eqs. (84) and (86) of Ref. [34], we calculate the baryon asymmetry represented by the ratio of the net baryon number $a_R^3 n_B^R$ (98) to the entropy S_R . Per comoving volume, this ratio at the reheating a_R is given by

$$\frac{n_B^R}{s_R} = \frac{a_R^3 n_B^R}{S_R} \approx 1.46 \times 10^{-4} \frac{a_R^3 n_M^H(a_R)}{S_R} \approx 2.6 \times 10^{-4} \frac{T_{RH}}{\hat{m}}, \quad (99)$$

where the entropy $s_R = S_R/a_R^3$ at the genuine reheating. This result is consistent with the one derived from the processes of baryon-number violating decay, see Ref. [12]. This baryon number-to-entropy ratio n_B^R/s_R (99) preserves its value from the reheating to the present time. The present observational value is $n_B/s = 0.864_{-0.015}^{+0.016} \times 10^{-10}$ [4]. This determines the ratio of the reheating temperature T_{RH} and effective mass and degeneracy parameter \hat{m} ,

$$(T_{RH}/\hat{m}) \approx 3.3 \times 10^{-7}, \quad (100)$$

which is used to constrain the parameters $(g_Y^2/g_*^{1/2})$ and (\hat{m}/M_{pl}) , see Eq. (89) of Ref. [34], g_* is the effective degeneracy of relativistic particles $\bar{\ell}\ell$ produced in reheating.

C. Magnetogenesis via baryogenesis

We show how the magnetogenesis can be achieved via the baryogenesis in the scenario that the net baryon number creation is due to the horizon crossing of positive charged particle and negative charged antiparticle oscillations. Suppose that the Universe is spatially homogenous at the moment a_R of baryogenesis and reheating (91), the net particle number density $\delta n_M^{\text{crou}}t$ (94) is generated, consequently resulting in the net baryon number density n_B^R (98). These net baryons carry charges and its density n_B^R can generate an electric current density

$$\vec{j}_B \approx e \vec{v}_B n_B^R, \quad (101)$$

where e is the electron charge and the velocity \vec{v}_B represents the spacetime averaged relative velocity

$$\vec{v}_B \equiv \langle \delta \mathbf{v}_M \rangle = \langle \mathbf{v}_M^+ - \mathbf{v}_M^- \rangle / 2, \quad v_B \equiv |\langle \delta \mathbf{v}_M \rangle| \quad (102)$$

between the velocities of positive and negative charged particles, see Eq. (48). Provided the non-vanishing relative velocity $|\vec{v}_B| \neq 0$ and electric current density $|\vec{j}_B| \neq 0$, a nontrivial primordial magnetic field must be generated and frozen inside the horizon, associating to the net baryon number density n_B^R (98).

Denote that inside the horizon at the reheating, B_R represents the primordial magnetic field in the coordinate frame. In order to estimate the upper and lower limits of the primordial magnetic field B_R , we use the integral form of the Maxwell equation,

$$\oint_{\ell_R} \vec{B}_R \cdot d\vec{\ell} = 4\pi \oint_{\mathcal{A}_R} \vec{j}_B \cdot d\vec{\sigma}, \quad (103)$$

where the area $\mathcal{A}_R = \pi H_{\text{RH}}^{-2}$ and its boundary $\ell_R = 2\pi H_{\text{RH}}^{-1}$ inside the horizon.

1. Upper limit of primordial magnetic fields

In the reheating epoch of high temperature, positively and negatively charged particles are ultra-relativistic and their velocities $\mathbf{v}_M^\pm \approx 1$ are about the speed of light. Suppose an extreme situation that the directions and values of relative velocities of positively and negatively charged particles in the expanding spacetime is “orderly” distributed, so that the relative velocity $|\vec{v}_B| = 1$. This situation gives the upper limit of the primordial magnetic field B_R at the genuine reheating,

$$B_R(2\pi)H_{\text{RH}}^{-1} < \pi H_{\text{RH}}^{-2}(4\pi e)n_B^R(a_R). \quad (104)$$

As a result, by using the net baryon number density n_B^R (98), we obtain in the unit of the critical field value $B_c = m_e^2/e \approx 4 \times 10^{14}$ Gauss

$$\begin{aligned} \frac{B_R}{B_c} &< \frac{2\pi\alpha}{m_e^2 H_{\text{RH}}} 1.46 \times 10^{-4} n_B^R(a_R) \\ &\approx 1.46 \times 10^{-4} (2\pi\alpha\chi) \frac{\hat{m} H_{\text{RH}}^2}{m_e^2 H_{\text{RH}}}, \end{aligned} \quad (105)$$

where m_e is the electron mass and α is the fine structure constant. Further adopting the reheating scale H_{RH} (89) and the relation (T_{RH}/\hat{m}) (100), the upper limit of the primordial magnetic field at the reheating is obtained

$$\frac{B_R}{B_c} < 3.89 \times 10^{-7} \left(\frac{8\pi g_*}{90} \right)^{1/2} \left(\frac{\hat{m}}{m_e} \right)^2 \left(\frac{\hat{m}}{M_{\text{pl}}} \right) \left(\frac{T_{\text{RH}}}{\hat{m}} \right)^2 \quad (106)$$

$$B_R < 3.4 \times 10^{40} \left(\frac{g_*}{90} \right)^{1/2} \left(\frac{\hat{m}}{M_{\text{pl}}} \right)^3 \text{ Gauss.} \quad (107)$$

This result depends on the ratio (\hat{m}/M_{pl}) in terms of the tensor-to-scalar ratio r , see Figure 10 (left) of Ref. [34].

By the total magnetic flux conservation from the Maxwell Equation $\vec{\nabla} \cdot \vec{B} = 0$, the primordial magnetic field reduces to its present value $B_0 = (a_R/a_0)^2 B_R$ [10]. As a result, we obtain the upper limit of the primordial magnetic field observed at the present time,

$$B_0 = (a_R/a_0)^2 B_R < 3.4 \times 10^{-14} \left(\frac{g_*}{90}\right)^{1/2} \left(\frac{\hat{m}}{M_{\text{pl}}}\right)^3 \text{ Gauss} \quad (108)$$

where $a_R/a_0 = (g_*/2)^{1/3}(T_{\text{TH}}/T_{\text{CBM}})$, see Eq. (82) of Ref. [34]. Using the reheating $T_{\text{RH}} \sim 10^{15}\text{GeV}$, the radiation-matter equilibrium temperature $T_{\text{eq}} \sim 10 \text{ eV}$ and the entropy conservation $T_{\text{RH}}a_R \approx T_{\text{eq}}a_{\text{eq}}$, we estimate $(a_R/a_0) = (a_R/a_{\text{eq}})(a_{\text{eq}}/a_0) \sim 10^{-23} \times 10^{-4} \sim 10^{-27}$, where a_{eq} and a_0 are the scale factors at the radiation-matter equilibrium and the present time. Considering $g_* \sim 10^2$ for the SM particle physics and $(\hat{m}/M_{\text{pl}}) \approx 5$ for $r \approx 0.044$ in Figure 10 (left) of Ref. [34], we obtain $B_0 < 4.48 \times 10^{-12}\text{G}$, consistently with the observed upper limit $B_{1\text{Mpc}}^{\text{prim}} < 10^{-9}\text{G}$ [8]. On the other hand, this observed upper limit $B_{1\text{Mpc}}^{\text{prim}} < 10^{-9}\text{G}$ implies the ratio $(\hat{m}/M_{\text{pl}}) < 100$. This indicates the tensor-to-scalar ratio $r < 0.046$ from Figure 10 (left) of Ref. [34].

2. Lower limit of primordial magnetic fields

Another extremal situation is that the directions and values of relative velocities of positively and negatively particles in the reheating are ‘‘randomly’’ distributed, so that the relative velocity $|\vec{v}_B| = 0$ and the electric current density $|\vec{j}_B| = 0$ identically vanish in Eqs. (101) and (102). Therefore the primordial magnetic field B_R is exactly equal to zero. This could be the case, if all oscillating modes of positively and negatively charged particles were subhorizon size, i.e., no horizon crossing occurs. Instead, the relative velocity (102) should not vanish $|\vec{v}_B| \neq 0$ for the occurrence of horizon crossing of particle-antiparticle oscillating modes, which leads to the non-vanishing asymmetric density perturbation $\delta n_M^{\text{crou}} \propto \bar{\delta}_M^{\text{crou}}$ (93) and the net baryon number density n_B^R in the genuine reheating. The reason for $|\vec{v}_B| \neq 0$ is similar to that for the non-vanishing asymmetric density perturbation $\bar{\delta}_M^{\text{crou}} \neq 0$ at the horizon crossing.

We can approximately calculate this value of the relative velocity $|\vec{v}_B| \neq 0$ from Eqs. (52) and (102), yielding

$$\begin{aligned} \nabla \cdot \delta \mathbf{v}_M &= -(\dot{\delta}_M^+ - \dot{\delta}_M^-) - \Gamma_M(\delta_M^+ - \delta_M^-) \\ &= -d\bar{\delta}_M/dt - \Gamma_M\bar{\delta}_M = -\Gamma_M\bar{\delta}_M, \end{aligned} \quad (109)$$

and the second line is evaluated on the horizon where the mode amplitude $\bar{\delta}_M$ (79) is frozen as a constant and $d\bar{\delta}_M/dt = 0$. By using the Gauss law for the spherically symmetric case, the approximate value $|\delta\mathbf{v}_M|$ on the horizon surface can be found

$$|\delta\mathbf{v}_M|_{\min} = \frac{4\pi H^{-3} \Gamma_M \bar{\delta}_M^{\text{crou}}}{3} = \frac{\Gamma_M \bar{\delta}_M^{\text{crou}}}{3H} \approx \frac{2}{3} \bar{\delta}_M^{\text{crou}}, \quad (110)$$

that is evaluated at the superhorizon crossing $H_{\text{crou}} = \Gamma_M^{\text{crou}}/2$ (90), close to the genuine reheating $H_{\text{RH}} \approx \Gamma_M^{\text{de}}/2$. The asymmetric pair density perturbation $\bar{\delta}_M^{\text{crou}} = 2.31 \times 10^{-4}$ (92) at the superhorisopn crossing. This small value of the relative velocity $|\vec{v}_B| = |\delta\mathbf{v}_M|_{\min}$ (110) gives rise to the lower limit of primordial magnetic fields generated in reheating.

Following the same calculations for the upper limit and replacing $|\vec{v}_B| = 1$ by $|\vec{v}_B| = |\delta\mathbf{v}_M|_{\min}$, we obtain the lower limit of primordial magnetic fields generated at reheating

$$B_R > 5.24 \times 10^{36} \left(\frac{g_*}{90}\right)^{1/2} \left(\frac{\hat{m}}{M_{\text{pl}}}\right)^3 \text{ Gauss}, \quad (111)$$

and at the present time,

$$B_0 = (a_R/a_0)^2 B_R > 5.24 \times 10^{-18} \left(\frac{g_*}{90}\right)^{1/2} \left(\frac{\hat{m}}{M_{\text{pl}}}\right)^3 \text{ Gauss}. \quad (112)$$

Using the same range of parameters for the upper limit case: $g_* \sim 10^2$ for the Standard Model of elementary particle physics and $(\hat{m}/M_{\text{pl}}) \approx 5$ for $r \approx 0.044$ in Figure 10 (left) of Ref. [34], we obtain $B_0 > 6.9 \times 10^{-16} \text{G}$, consistently with the observed lower limit $B_{>1\text{Mpc}} > 10^{-17} \text{G}$ [7]. As a preliminary result, the theoretical lower and upper limits of primordial magnetic fields generated at reheating

$$4.48 \times 10^{-12} > B_0 > 6.9 \times 10^{-16} \text{ Gauss}. \quad (113)$$

These are very crude upper and lower limits, since they depend on the scale factor $(a_R/a_0)^2$, the effective degeneracy g_* of relativistic particles and the the effective mass and degeneracy of massive pairs (\hat{m}/M_{pl}) . However, what we can be sure is the existence of the upper and lower limits of the primordial magnetic field from the point view of its generation in this theoretical scenario.

IX. DARK-MATTER ACOUSTIC WAVE AND LARGE-SCALE STRUCTURE

In Sec. V, we describe the pair-density oscillations and particle-antiparticle density oscillations. Our attention is focused on the “zero mode” $|\mathbf{k}| = 0$ oscillations δ_M^0 and Δ_M^0 of the frequency $\omega = (2H\Gamma)^{1/2}$ in Sec. VI and their horizon crossing in Sec VII, as well as physical consequences for the baryogenesis and magnetogenesis in Secs VIII and VIII C.

In this section, we shall discuss other oscillating modes $\delta_M^{\mathbf{k}}$ and $\Delta_M^{\mathbf{k}}$ ($|\mathbf{k}| \neq 0$) of the frequencies $\omega_{\delta,\Delta}(|\mathbf{k}|)$ (63) and (64). In particular, for the modes $\Delta_M^{\mathbf{k}}$, we examine the negative term $4\pi G\rho_M^H \Delta_M^{\mathbf{k}}$ in the frequency $\omega_{\Delta}(|\mathbf{k}|)$ (64) to study the Jeans instability in both (a) the pre-inflationary epoch where $m \gtrsim H$ and $v_s^2 \lesssim 1$, namely pairs can be relativistic; and (b) the inflationary epoch where $m \gg H$ and $v_s^2 \ll 1$, namely pairs are non relativistic. Note that the effective pair mass and degeneracy parameter m is generally assigned for the pre-inflation, and $m = m_*$ has been used for the inflation, they are different from the one $m = \hat{m}$ for the reheating. To be specific, we turn to study the non-zero modes $\delta_M^{\mathbf{k}}$ and $\Delta_M^{\mathbf{k}}$ ($|\mathbf{k}| \neq 0$) to see:

- (i) their superhorizon crossings at $\omega_{\delta,\Delta}(|\mathbf{k}|) \approx H$ in the pre-inflation and inflation epochs;
- (ii) their subhorizon crossings at large length scales, yielding peculiar “dark-matter” sound waves imprinting on the matter power spectrum at large scale lengths;
- (iii) any possible impact on the formation of large-scale structure,

and we present qualitative analysis and discussions, as well as speculations.

To start with, we would like to emphasise that the oscillations (perturbations) discussed here are the kinds of sound waves of the dispersion relations (63) and (64), due to fluctuations in the form of the local equation of state $\omega_M = v_s^2$ (54) of particles and antiparticles, namely spacial fluctuations in the number of particles or antiparticles (compositions) per comoving volume. This is different from the curvature perturbations as fluctuations in energy density characterised as fluctuations in the local value of the spatial curvature of the spacetime.

A. Pair-density and particle-antiparticle-density perturbations

The “non-zero” modes are described by the comoving momentum $|\mathbf{k}|$ (wavelength $\lambda = |\mathbf{k}|^{-1}$), whose value is constant in time. As a reference, we consider the pivot scale $k^* = 0.05(\text{Mpc})^{-1}$, at which the curvature perturbations cross outside and inside horizons twice, accounting for the CMB observations. The corresponding values of the horizon $k^* = (Ha)_*$, the ϵ -rate $\epsilon = \epsilon^*$ and the effective mass parameter $m = m_*$ are given by Eqs. (9) and (10).

The case $|\mathbf{k}| > k^*$ corresponds to the modes that exit the horizon in the pre-inflation epoch and reenter the horizon after the recombination epoch. The case $|\mathbf{k}| < k^*$ corresponds to the modes that exit the horizon in the inflation epoch and reenter the horizon before the recombination epoch.

In both cases, $H \gg \Gamma_M = (\chi/4\pi)m\epsilon$ and $\epsilon \ll 1$. Equations (61) and (62) approximately become,

$$\ddot{\delta}_M^{\mathbf{k}} + 2H\dot{\delta}_M^{\mathbf{k}} \approx -\omega_\delta^2(|\mathbf{k}|)\delta_M^{\mathbf{k}}, \quad (114)$$

$$\ddot{\Delta}_M^{\mathbf{k}} + 2H\dot{\Delta}_M^{\mathbf{k}} \approx -\omega_\Delta^2(|\mathbf{k}|)\Delta_M^{\mathbf{k}}, \quad (115)$$

where the Hubble rate H slowly varies $H \approx \text{const.}$ Following the same discussions in previous Sec. VI or the discussions of the usual curvature perturbations, these non-zero modes $\delta_M^{\mathbf{k}}$ and $\Delta_M^{\mathbf{k}}$ of $|\mathbf{k}| \neq 0$ cross horizon from the subhorizon to the superhorizon at $\omega_{\delta,\Delta}(|\mathbf{k}|) = 2H$ (72), yielding

$$|\mathbf{k}|_{\delta_{\text{cross}}}^2 = \left(4 - \chi \frac{\epsilon_\Lambda m}{2\pi H}\right) \frac{(Ha)^2}{v_s^2} \Big|_{\text{cross}} \approx 4 \frac{(Ha)^2}{v_s^2} \Big|_{\text{cross}}, \quad (116)$$

$$\begin{aligned} |\mathbf{k}|_{\Delta_{\text{cross}}}^2 &= \left[4 - \chi \frac{\epsilon_\Lambda m}{2\pi H} + \chi \left(\frac{m}{m_{\text{pl}}}\right)^2\right] \frac{(Ha)^2}{v_s^2} \Big|_{\text{cross}} \\ &\approx 4 \frac{(Ha)^2}{v_s^2} \Big|_{\text{cross}}, \end{aligned} \quad (117)$$

for the both the pre-inflation epoch $H \lesssim m$ and the inflation epoch $H \ll m$. These results depend on the sound velocity v_s value, which needs numerical calculations.

The horizon crossing (116) and (117) show that because of $v_s^2 < 1$, the modes $|\mathbf{k}|_{\delta_{\text{cross}},\Delta_{\text{cross}}} > k^*$ cross the horizon before the inflation start $k^* = (Ha)_*$, and reenter the horizon after the recombination $(Ha)_*$. Therefore, it is impossible that these sound-wave perturbations cross outside the horizon in the inflation epoch, then cross inside the horizon before recombination. Whereas, it is possible that the sound-wave perturbations cross outside the horizon in the pre-inflation epoch, then cross inside the horizon after the recombination. Moreover, the ‘‘non-zero’’ modes of larger $|\mathbf{k}|_{\delta_{\text{cross}},\Delta_{\text{cross}}}$ exit the horizon earlier and reentry the horizon later, therefore these sound-wave modes should leave their imprints on the linear regime of large-scale structure and the nonlinear regime of galaxy clustering. Among particle and antiparticle pairs produced from the spacetime, it is conceivable there are mainly dark-matter particles, we called these acoustic modes ‘‘dark-matter’’ sound waves [33], which will be discussed in some details below.

B. Pair-density perturbation and large-scale structure

The particle-antiparticle symmetric modes $\Delta_M^{\mathbf{k}}$ (56) represent the acoustic waves of pair-density perturbations of the dispersion relation (64), analogously to the matter density perturbation wave in gravitation fields. We examine the dispersion relation (64) to see whether the Jeans instability occurs and the $\Delta_M^{\mathbf{k}}$ amplitudes are amplified for imaginary frequencies $\omega_\Delta^2(|\mathbf{k}|) < 0$, i.e.,

$$|\mathbf{k}|_\Delta^2 < |\mathbf{k}|_{\text{Jeans}}^2 \equiv \chi \left[\left(\frac{m}{m_{\text{pl}}}\right)^2 - \frac{\epsilon_\Lambda m}{2\pi H} \right] \frac{(Ha)^2}{v_s^2}, \quad (118)$$

where $|\mathbf{k}|_{\text{Jeans}}$ is the Jeans wavenumber and wavelength $\lambda_{\text{Jeans}} = |\mathbf{k}|_{\text{Jeans}}^{-1}$. The modes $\Delta_M^{\mathbf{k}}$ of wavelengths $\lambda > \lambda_{\text{Jeans}}$ undergo the Jeans instability due to the prevail of gravitational attraction of pair-density perturbations.

In the inflation epoch, the gravitational attractive term $4\pi G\rho_M^H$ is negligible compared with the term $2H\Gamma_M$ in the frequency ω_Δ^2 (64), thus $\omega_\Delta^2 > 0$ and the Jeans instability does not occur. In the pre-inflation epoch, instead, the term $2H\Gamma_M$ is negligible compared with the gravitational attractive term $4\pi G\rho_M^H$. It is then possible to have the imaginary frequency (63) $\omega_\Delta^2 < 0$ for $|\mathbf{k}|_\Delta^2 < |\mathbf{k}|_{\text{Jeans}}^2$ (118), where

$$|\mathbf{k}|_{\text{Jeans}}^2 \approx \chi \left(\frac{m}{m_{\text{pl}}} \right)^2 \frac{(Ha)^2}{v_s^2}; \quad \chi \left(\frac{m}{m_{\text{pl}}} \right)^2 < 1, \quad (119)$$

and the Jeans instability could occur.

1. Stable modes and dark-matter sound waves

For short-wavelength modes $|\mathbf{k}|_\Delta^2 > |\mathbf{k}|_{\text{Jeans}}^2$, the pressure terms ($v_s^2|\mathbf{k}|^2/a^2$) are dominant in the frequency ω_Δ^2 (64), compared with the gravitational attraction $4\pi G\rho_M^H$ of pair-density perturbations. Equation (115) for the pair-density perturbation approximately becomes

$$\ddot{\Delta}_M^{\mathbf{k}} + 2H\dot{\Delta}_M^{\mathbf{k}} = -(v_s^2|\mathbf{k}|^2/a^2)\Delta_M^{\mathbf{k}}, \quad (120)$$

which is the typical Mukhanov-Sasaki equation, similarly to the one for the curvature perturbation. Its solution can be found by using Eqs. (68), (69) and (70),

$$\Delta_M^{\mathbf{k}}(t) \propto e^{-Ht} \exp -i\tilde{\omega}_\Delta(|\mathbf{k}|)(1 - \zeta^2)^{1/2}t, \quad \zeta \approx \frac{H}{\tilde{\omega}_\Delta(|\mathbf{k}|)} = \frac{Ha}{v_s|\mathbf{k}|_\Delta}, \quad (121)$$

where the sound-wave frequency $\tilde{\omega}_\Delta(|\mathbf{k}|) = v_s|\mathbf{k}|_\Delta/a$.

For the given comoving horizon (Ha) and the sound velocity v_s , the horizon crossing wavenumber $|\mathbf{k}|_{\Delta\text{cross}} = 2Ha/v_s$ (117) is larger than the Jeans wavenumber $|\mathbf{k}|_{\text{Jeans}}$ (119), i.e.,

$$|\mathbf{k}|_{\Delta\text{cross}} > |\mathbf{k}|_{\text{Jeans}}. \quad (122)$$

This shows that the pair-density perturbations $\Delta_M^{\mathbf{k}}$ oscillate as

- (i) *sub-horizon sized modes*: an underdamped sound wave inside the horizon for $\zeta < 1$ and $|\mathbf{k}|_\Delta > |\mathbf{k}|_{\Delta\text{cross}} > |\mathbf{k}|_{\text{Jeans}}$, the modes $\Delta_M^{\mathbf{k}}(t)$ are stable oscillating modes;
- (ii) *super-horizon sized modes*: an overdamped sound wave outside the horizon for $\zeta > 1$ and $|\mathbf{k}|_{\text{Jeans}} < |\mathbf{k}|_\Delta < |\mathbf{k}|_{\Delta\text{cross}}$, the mode amplitudes $\Delta_M^{\mathbf{k}} \propto \text{const}$ are frozen.

On the other hand, as the comoving horizon (Ha) increases and the sound velocity v_s decreases in the pre-inflation epoch [33], the horizon crossing wavenumber $|\mathbf{k}|_{\Delta_{\text{cross}}}$ (117) increases. The mode $\Delta_M^{\mathbf{k}}$ of a fixed wavenumber $|\mathbf{k}|_{\Delta}$ evolves from the *sub-horizon sized mode* to *super-horizon sized modes*, and the horizon crossing occurs at $|\mathbf{k}|_{\Delta} = |\mathbf{k}|_{\Delta_{\text{cross}}}$ (117).

Moreover, the *super-horizon sized mode* $|\mathbf{k}|_{\Delta}$ reenters the horizon at the horizon $(Ha)_{\text{reenter}}$ and becomes a *sub-horizon sized mode*, when

$$|\mathbf{k}|_{\Delta} = (Ha)_{\text{reenter}}, \quad (123)$$

where $(Ha)_{\text{reenter}}^{-1}$ is the comoving horizon size after the recombination. This mode $|\mathbf{k}|_{\Delta} = (Ha)_{\text{reenter}}$ behaves as a sound wave of the dark-matter density perturbations, imprinting on the matter power spectrum of low- ℓ multipoles $\ell \leq 2$, corresponding to large length scales. This is reminiscent of baryon acoustic oscillations due to the coupling in the baryon-photon fluid.

These are qualitative discussions on the dark-matter sound waves, that are expected to be possibly relevant for observations. However, the quantitative results depend not only on the initial amplitude value $\Delta_M^{\mathbf{k}}(0)$, the wavenumber $|\mathbf{k}|_{\Delta}$ and the horizon crossing size (Ha) , but also on the sound velocity v_s in Eq. (121).

2. Unstable modes and large-scale structure

For long-wavelength modes $|\mathbf{k}|_{\Delta}^2 \ll |\mathbf{k}|_{\text{Jeans}}^2$, the pressure terms ($v_s^2|\mathbf{k}|^2/a^2$) are negligible in the frequency ω_{Δ}^2 (64), compared with the gravitational attraction $4\pi G\rho_M^H$ of pair-density perturbations. Equation (115) for the pair-density perturbation approximately becomes

$$\ddot{\Delta}_M^{\mathbf{k}} + 2H\dot{\Delta}_M^{\mathbf{k}} = \chi\left(\frac{m}{m_{\text{pl}}}\right)^2 H^2 \Delta_M^{\mathbf{k}}, \quad (124)$$

as the microscopic physics (e.g., pressure terms ($v_s^2|\mathbf{k}|^2/a^2$)) are impotent and negligible, where the Hubble rate H is approximately a constant, very slowly varies in the pre-inflation epoch.

Equation (124) is a new kind of differential equation for perturbations, differently from Eq. (120) of the Mukhanov-Sasaki type. This equation (124) has two independent solutions:

$$\Delta_M^{\mathbf{k}}(t) \propto \exp -2Ht; \quad \Delta_M^{\mathbf{k}}(t) \propto \exp + \frac{\chi H}{2} \left(\frac{m}{m_{\text{pl}}}\right)^2 t. \quad (125)$$

At late times, the exponentially glowing modes of pair-density perturbation are important, whereas the exponentially decaying modes physically correspond to a perturbation with initial overdensity and velocity arranged so that the initial velocity perturbation eventually eases the pair-density perturbation.

Equation (119) shows that $|\mathbf{k}|_{\Delta}^2 \ll |\mathbf{k}|_{\text{Jeans}}^2$ means $|\mathbf{k}|_{\Delta}^2 < |\mathbf{k}|_{\Delta\text{cross}}^2$, indicating these modes (125) are superhorizon size. This is consistent with neglecting the pressure term ($v_s^2|\mathbf{k}|^2/a^2$) of the microscopic physics, that cannot causally arrange the pair-density perturbations in superhorizon size. As a result, the gravitational attraction is not balanced by the pressure terms, leading to increase the amplitudes of pair-density perturbations. These unstable and super-horizon sized modes (125) exponentially grow in time and the characteristic time scale is

$$\tau_{\Delta}^{-1} = \frac{\chi H}{2} \left(\frac{m}{m_{\text{pl}}} \right)^2. \quad (126)$$

These solutions (modes) are very different from the super-horizon sized modes of frozen constant amplitudes (70) or (121) for $\zeta \gg 1$. We consider such an unstable and super-horizon sized mode of fixed wavenumber $|\mathbf{k}|_{\Delta}$, which satisfies

$$|\mathbf{k}|_{\text{Jeans}} > |\mathbf{k}|_{\Delta} > k^*, \quad (127)$$

where $|\mathbf{k}|_{\Delta\text{cross}} > |\mathbf{k}|_{\text{Jeans}}$ (122) and k^* is the pivot scale of CMB observations. Although the initial amplitude $\Delta_M^{\mathbf{k}}(0)$ of such a mode (125) is very small, as the curvature perturbations, it could be greatly amplified in the super horizon, before the mode reenters the sub horizon. Therefore, it is possible that such mode $\Delta_M^{\mathbf{k}}$ of the pair-density perturbation is no longer a small perturbation, when its wavelength $|\mathbf{k}|_{\Delta}^{-1}$ become sub-horizon sized, $|\mathbf{k}|_{\Delta} = (Ha)_{\text{reenter}}$ (124), crossing the horizon after the recombination $(Ha)_{\text{reenter}} < (Ha)_*$. This phenomenon can possibly plays some physical roles in the formations of large-scale structure and galaxy cluster.

We recall the basic scenario of primordial curvature perturbations leading to the large-scale structure in the standard cosmology. The curvature perturbations, whose amplitudes are small constants in superhorizon, reenter the horizon and lead to the CMB temperature anisotropic fluctuation $\delta T/T \sim \mathcal{O}(10^{-5})$. These fluctuations relate to the matter density perturbations $\delta\rho/\rho \propto \delta T/T \sim \mathcal{O}(10^{-3})$ at the recombination of the redshift $z \sim 10^3$. These matter density perturbations (amplitudes) are small and their physical sizes (wavelengths) increase linearly as the scale factor $a(t)$. However under the influences of their gravitational attractions and the Jeans instability, the matter density perturbations glow $\delta\rho/\rho \propto \mathcal{O}(1)$ and become nonlinear, therefore approximately maintain constant physical sizes, eventually forming the large-scale structure.

In addition to the curvature perturbations, our qualitative analysis and discussions imply that the pair-density perturbations, when they reenter the horizon after the recombination and their amplitudes are amplified in the superhorizon up to the order of unity $\Delta_M^{\mathbf{k}} \propto \mathcal{O}(1)$, should have some physical consequences on the formation of large scale structure and galaxies. However, we are not able to give quantitative results in this article and further studies are obviously required.

C. Particle-antiparticle density perturbations and “plasma” acoustic wave

We turn to the discussions of the particle-antiparticle density perturbations $\delta_M^{\mathbf{k}}$, described by the frequency $\omega_\delta(\mathbf{k})$ (63) and oscillating equation (114),

$$\ddot{\delta}_M^{\mathbf{k}} + 2H\dot{\delta}_M^{\mathbf{k}} = -(v_s^2|\mathbf{k}|^2/a^2)\delta_M^{\mathbf{k}}, \quad (128)$$

and horizon crossing (117). These are the same as those for the pair-density perturbations $\Delta_M^{\mathbf{k}}$, except the absence of the gravitational attraction term $4\pi G\rho_M^H$ and Jeans instability. The solution is similar to the stable $\Delta_M^{\mathbf{k}}$ modes (121)

$$\delta_M^{\mathbf{k}}(t) \propto e^{-Ht} \exp -i\tilde{\omega}_\delta(|\mathbf{k}|)(1 - \zeta^2)^{1/2}t, \quad \zeta \approx \frac{H}{\tilde{\omega}_\delta(|\mathbf{k}|)} = \frac{Ha}{v_s|\mathbf{k}|_\delta}, \quad (129)$$

where the sound-wave frequency $\tilde{\omega}_\delta(|\mathbf{k}|) = v_s|\mathbf{k}|_\delta/a$. For the given comoving horizon (Ha) and the sound velocity v_s , the horizon crossing wavenumber $|\mathbf{k}|_{\delta\text{cross}} = 2Ha/v_s$ (116). This shows that the particle-antiparticle density perturbations $\delta_M^{\mathbf{k}}$ oscillate as

- (i) *sub-horizon sized modes*: an underdamped sound wave inside the horizon for $\zeta < 1$ and $|\mathbf{k}|_\delta > |\mathbf{k}|_{\delta\text{cross}}$, the modes $\delta_M^{\mathbf{k}}(t)$ are stable oscillating modes;
- (ii) *super-horizon sized modes*: an overdamped sound wave outside the horizon for $\zeta > 1$ and $|\mathbf{k}|_\delta < |\mathbf{k}|_{\delta\text{cross}}$, the mode amplitudes $\delta_M^{\mathbf{k}} \propto \text{const}$ are frozen.

On the other hand, as the comoving horizon (Ha) increases and the sound velocity v_s decreases in the pre-inflation epoch, the horizon crossing wavenumber $|\mathbf{k}|_{\delta\text{cross}}$ (116) increases. The mode $\delta_M^{\mathbf{k}}$ of a fixed wavenumber $|\mathbf{k}|_\delta$ evolves from a *sub-horizon sized mode* to a *super-horizon sized mode*, and the horizon crossing occurs at $|\mathbf{k}|_\delta = |\mathbf{k}|_{\delta\text{cross}}$ (116). Moreover, the *super-horizon sized mode* $|\mathbf{k}|_\delta$ reenters the horizon at the horizon $(Ha)_{\text{reenter}}$, when

$$|\mathbf{k}|_\delta = (Ha)_{\text{reenter}}, \quad (130)$$

after the recombination, and it becomes a *sub-horizon sized mode* again.

The modes $|\mathbf{k}|_\delta = (Ha)_{\text{reenter}}$ of the particle-antiparticle density perturbations $\delta_M^{\mathbf{k}}$ (56) represent the acoustic waves of particle and antiparticle oscillations of the dispersion relation (63), analogously to the neutral plasma oscillations of electrons and positrons. They respect the symmetry of particles and antiparticles. These modes exit the horizon in the pre-inflation epoch and reenter the horizon after the recombination. This implies that such acoustic waves from the primordial Universe would leave their imprints on the Universe after the recombination, possibly imprinting

on the matter power spectrum of low- ℓ multipoles $\ell \leq 2$, corresponding to large length scales. However, we expect that the mode amplitudes $\delta_M^{\mathbf{k}}$ should be small, given the energy densities ρ_M^+ and ρ_M^- of particles and antiparticles, namely the pair energy density $\rho_M^H = \rho_M^+ + \rho_M^-$ and $\rho_M^+ = \rho_M^-$, are small in the pre-inflation epoch.

In this section, we qualitatively describe three types of “dark-matter” sound waves originated from the particle-antiparticle oscillations on the horizon in the pre-inflation epoch: (i) stable pair-density perturbations; (ii) unstable pair-density perturbations; (iii) particle-antiparticle density perturbations, and present some discussions on their returns to the horizon after the recombination and possible relevances for observations. However, we cannot give quantitative results that depend not only on the perturbation modes’ wavenumbers $|\mathbf{k}|_{\Delta,\delta}$, initial amplitude values $\Delta_M^{\mathbf{k}}(0)$ and $\delta_M^{\mathbf{k}}(0)$, and the sound velocity v_s in their oscillating equations (120) and (128), but also on the horizon crossing size $(Ha)^{-1}$ (116) and (117).

X. SUMMARY AND REMARKS

The article mainly consists of three studies of issues: baryogenesis, magnetogenesis, and dark-matter acoustic waves. We conclude this lengthy article by briefly summarising fundamental equations adopted, basic physical phenomena described and results obtained that gives some insight into these three issues.

We use Einstein (Friedmann) equations (1) and (2), together with the cosmic rate equation (20), and reheating equation (22) for the massive pair decay $\bar{F}F \Rightarrow \bar{\ell}\ell$, as well as the pair-production rate (7) and pair-decay rate (19), so as to completely determine the time-varying horizon H , cosmological term Ω_Λ , matter term Ω_M and radiation term Ω_R in the reheating. We apply this complete set of independent ordinary differential equations (23-26) to calculate the horizon H variation in complex reheating epoch: (i) the preheating \mathcal{P} -episode; (ii) massive pairs oscillating domination \mathcal{M} -episode; (iii) relativistic particles domination \mathcal{R} -episode of the genuine reheating.

The perturbations of massive particle and antiparticle densities on the cosmic evolving horizon H are important and peculiar issue studied in this article. Starting from Eqs. (44-47) for the density perturbations of particles and antiparticles, we derive the acoustic wave equations (61-62) for the particle-antiparticle symmetric pair-density perturbation Δ_M (55) and the particle-antiparticle asymmetric density perturbation δ_M (56). We study their lowest lying modes of zero wavenumbers $|\mathbf{k}|_{\Delta,\delta} = 0$, and how they enter the horizon from superhorizon to subhorizon (83) in the preheating episode, then exit the horizon from subhorizon to superhorizon (88) in the genuine reheating

episode. It is due to a such phenomenon that the particle-antiparticle asymmetric density perturbations δ_M undergo horizon crossing in the genuine reheating episode, the net number density (94) of particle and antiparticle is generated inside the horizon, leading to the baryogenesis phenomenon. We compute the baryon number-to-entropy ratio, and the result (99) is in agreement with the observed result. Moreover, attributed to the net electric current produced by the baryogenesis, the magnetogenesis phenomenon takes place. From purely theoretical view points, we determine the maximal and minimal values of the net electric current. Thus we use the Maxwell equation to estimate lower and upper bounds of primeval magnetic fields, the results are consistent with the current observational constrains.

In addition, we study the acoustic modes ($|\mathbf{k}|_{\Delta,\delta} \neq 0$) of the pair-density perturbation $\Delta_M^{\mathbf{k}}$ (115) and the particle-antiparticle asymmetric density perturbation $\delta_M^{\mathbf{k}}$ (114), and show how they become superhorizon sized modes (116) and (117) in the pre-inflation epoch, then return to the horizon $|\mathbf{k}|_{\Delta,\delta} = (Ha)_{\text{reenter}}$ after the recombination. These modes behave as sound waves of “dark-matter” density perturbations or particle-antiparticle oscillating perturbations, possible leaving some imprints on the matter power spectrum of low- ℓ multipoles $\ell \leq 2$, corresponding to large length scales. Due to the gravitational attraction of the pair-density perturbation $\Delta_M^{\mathbf{k}}$ (124), possibly leading to the Jeans instability, the tiny amplitudes $\Delta_M^{\mathbf{k}}$ of unstable superhorizon sized modes can get amplified. When they reenter the horizon after the recombination, these unstable modes of pair-density perturbations are of the order of unity $\Delta_M^{\mathbf{k}} \propto \mathcal{O}(1)$, rather than very tiny $\Delta_M^{\mathbf{k}} \ll \mathcal{O}(1)$. As a consequence, they should have some physical influences on the formation of large scale structure and galaxies, which need further investigations. It would be worthwhile and interesting to study whether these unstable and Jeans-amplified pair-density perturbations $\Delta_M^{\mathbf{k}}$ produce primordial gravitational waves.

Further studies are still required and more elaborately numerical computations are very inviting. Nevertheless, we expect that this theoretical scenario and present results give some insights into the baryogenesis and magnetogenesis phenomena, and the prevision of “dark matter” acoustic waves in Universe evolution.

XI. ACKNOWLEDGMENT

Author thanks Drs. Yu Wang and Rahim Moradi for indispensable numerical assistances of using Python and mathematics.

-
- [1] A. H. Guth, Phys. Rev. D23, 347 (1981), [Adv. Ser. Astrophys. Cosmol.3,139(1987)].
 A. D. Linde, QUANTUM COSMOLOGY, Phys. Lett. 108B, 389 (1982), [Adv. Ser. Astrophys. Cosmol.3,149(1987)].
 A. Albrecht and P. J. Steinhardt, Phys. Rev. Lett. 48, 1220 (1982), [Adv. Ser. Astrophys. Cosmol.3,158(1987)].
 A. D. Linde, Phys. Lett. 129B, 177 (1983).
 Y. Akrami et al. (Planck), (2018), arXiv:1807.06211 [astro-ph.CO].
- [2] M. A. Amin, M. P. Hertzberg, D. I. Kaiser, and J. Karouby, Int. J. Mod. Phys. D24, 1530003 (2014), arXiv:1410.3808 [hep-ph].
 R. Allahverdi, R. Brandenberger, F.-Y. Cyr-Racine, and A. Mazumdar, Ann. Rev. Nucl. Part. Sci. 60, 27 (2010), arXiv:1001.2600 [hep-th].
 Peter Adshead, John T. Giblin Jr, Mauro Pieroni, Zachary J. Weiner, Phys. Rev. Lett. 124, 171301 (2020), <https://arxiv.org/abs/1909.12843>
 L. Kofman, A. D. Linde and A. A. Starobinsky, Phys. Rev. D 56, 3258 (1997).
 B. A. Bassett and S. Liberati, Phys. Rev. D 58, 021302 (1998) [Erratum-ibid. D 60, 049902 (1999)],
 S. Tsujikawa, K. i. Maeda and T. Torii, Phys. Rev. D60, 063515 (1999).
 D. I. Podolsky and A. A. Starobinsky, Grav. Cosmol. Suppl. 8N1, 13 (2002).
- [3] J. H. Traschen and R. H. Brandenberger, Phys. Rev. D42, 2491 (1990).
 Y. Shtanov, J. H. Traschen, and R. H. Brandenberger, Phys. Rev. D51, 5438 (1995), arXiv:hep-ph/9407247 [hep-ph]. L. Kofman, A. D. Linde, and A. A. Starobinsky, Phys. Rev. Lett. 73, 3195 (1994), arXiv:hep-th/9405187 [hep-th].
- [4] Planck Collaboration, “Planck 2015 results. XIII. Cosmological parameters, Astron. Astrophys. 594 (2016) A13, (arXiv1502.01589)
- [5] V.A.Kuzmin, V.A.Rubakov and M.E. Shaposhnikov, Physics Letters B155 (May 1985) 36.
 A. Dolgov and A. D. Linde, Phys. Lett. B116 (1982) 329.
 L. Abbott, E. Farhi and M. B. Wise, Phys. Lett. B117 (1982) 29.
 M. Dine and A. Kusenko, Rev. Mod. Phys. 76 (2004) 1, arXiv:hep-ph/0303065.
 J.M. Cline (2006) arXiv:hep-ph/0609145, Les Houches Summer School, Session86: Particle Physics and Cosmology: the Fabric of Spacetime, 7-11 Aug. 2006.
- [6] A. Dolgov and K. Freese, Phys. Rev. D51 (1995) 2693, arXiv:hep-ph/9410346 [hep-ph].

- A. Dolgov, K. Freese, R. Rangarajan and M. Srednicki, Phys.Rev. D56 (1997) 6155, arXiv:hep-ph/9610405 [hep-ph].
- J. Garcia-Bellido, D. Y. Grigoriev, A. Kusenko and M. E. Shaposhnikov, Phys. Rev. D60 (1999) 123504, arXiv:hep-ph/9902449 [hep-ph].
- S. Davidson, M. Losada and A. Riotto, Phys. Rev. Lett. 84 (2000) 4284, arXiv:hep-ph/0001301 [hep-ph].
- A. Megevand, Phys. Rev. D64 (2001) 027303, arXiv:hep-ph/0011019 [hep-ph].
- A. Tranberg and J. Smit, JHEP 0311 (2003) 016, arXiv:hep-ph/0310342 [hep-ph], JHEP 0608 (2006) 012, arXiv:hep-ph/0604263 [hep-ph].
- M. P. Hertzberg and J. Karouby, Phys. Rev. D89 (2014) 063523, arXiv:1309.0010 [hep-ph], Phys. Lett. B737 (2014) 34, arXiv:1309.0007 [hep-ph].
- M. P. Hertzberg, J. Karouby, W. G. Spitzer, J. C. Becerra and L. Li (2014), Phys. Rev. D 90, 123529 (2014) arXiv:1408.1398 [hep-th].
- Kaloian D. Lozanov and Mustafa A. Amin, Phys. Rev. D 90, 083528 (2014), <https://arxiv.org/pdf/1408.1811.pdf>.
- P. Hut and K. A. Olive, Phys. Lett. 87B, 144 (1979).
- S. Nussinov, Phys. Lett. 165B, 55 (1985).
- K. M. Zurek, Phys. Rept. 537, 91 (2014), [arXiv:1308.0338].
- [7] A. Kandus, K. E. Kunze, and C. G. Tsagas, Primordial magnetogenesis, Phys. Rept.505 (2011) 158, arXiv:1007.3891 [astro-ph.CO].
- [8] , Planck Collaboration, P. A. R. Ade et al., Planck 2015 results. XIX. Constraints on primordial magnetic fields, Astron. Astrophys. 594 (2016) A19, arXiv:1502.01594[astro-ph.CO].
- [9] P. P. Kronberg, Rept. Prog. Phys. 57 (1994) 325.
- K. Enqvist, International Journal of Modern Physics D 07 (1998) 331, <http://www.worldscientific.com/doi/pdf/10.1142/S0218271898000243>.
- A. Diaz-Gil, J. Garcia-Bellido, M. Garcia Perez and A. Gonzalez-Arroyo, Phys. Rev. Lett. 100 (2008) 241301, arXiv:0712.4263 [hep-ph], JHEP 0807, (2008) 043, arXiv:0805.4159 [hep-ph].
- [10] see for example, the review articles: D. Grasso and H.R. Rubinstein, “Magnetic Fields in the Early Universe”, Phys. Rept. 348:163-266,2001, arXiv:astro-ph/0009061
- K. Subramanian, “The origin, evolution and signatures of primordial magnetic fields”, Reports on Progress in Physics, Volume 79, Issue 7, article id. 076901 (2016), arXiv:1504.02311 .
- [11] P. J. E. Peebles, *Principles of Physical Cosmology*, Princeton: Princeton Univ. Press, 1993.
- [12] E. W. Kolb and M. S. Turner, “The Early Universe”, Published by Westview press, 1994.
- [13] For the review of inflation in effective theory, “Inflation and String theory”, D. Baumann and L. McAllister, Cambridge University Press (2015), ISBN 978-1-107-08969-3, and references there in.
- [14] Jerome Martin, Christophe Ringeval, Vincent Vennin, Phys. Dark Univ. 5-6 (2014) 75-235, (arXiv:1303.3787).

- [15] Cristiano Germani and Alex Kehagias, Phys. Rev. Lett. 105, 011302,2010, (arXiv:1003.2635).
- [16] Shuang Wang, Yi Wang, Miao Li, Physics Reports 696 (2017) 1-57, (arXiv:1612.00345); Miao Li, Xiaodong Li, Shuang Wang, Yi Wang, Commun. Theor. Phys. 56:525-604,2011 (arXiv:1103.5870); D. H. Lyth and A. Riotto, Phys. Rept. 314:1-146,1999 (arXiv:hep-ph/9807278v4).
- [17] K. Bamba, S. Capozziello, S. Nojiri and S. D. Odintsov, Astrophys. Space Sci. **342** (2012) 155 (arXiv:1205.3421).
- [18] S. Nojiri, S. D. Odintsov and V. K. Oikonomou, Phys. Rept. **692** (2017) 1 (arXiv:1705.11098).
- [19] A. A. Coley and G. F. R. Ellis, Class. Quant. Grav. v37 013001 (2020) (arXiv:1909.05346)
- [20] I. Prigogine, J. Gehehiau, E. Gunzig, P. Nardone, Gen. Rel. Grav. 21 (1989) 767-776.
- [21] S. K. Modak and D. Singleton, Phys. Rev. D86 (2012) 123515 ; e-Print: arXiv:1207.0230.
- [22] I. G. Dymnikova, M. Yu. Khlopov, Mod. Phys. Lett. A (2000) V. 15, PP. 2305-2314; arXiv:astro-ph/0102094. Eur. Phys. J. C (2001) V. 20, PP. 139-146.
- [23] B. Wang, E. Abdalla, F. Atrio-Barandela, D. Pavon, Reports on Progress in Physics 79 (2016) 096901, arXiv:1603.08299
- [24] Luis P. Chimento, Martn G. Richarte, Phys. Rev. D 86, 103501 (2012), <https://arxiv.org/abs/1210.5505>; The European Physical Journal C July 2013, 73:2497, <https://arxiv.org/abs/1308.0860>
- [25] Z.-P. Huang and Y.-L. Wu Phys. Rev. D85 (2012) 103007/ e-Print: arXiv:1202.4228
- [26] Y. Tang and Y.-L. Wu Phys. Lett. B784 (2018) 163-168, e-Print: arXiv:1805.08507.
- [27] Peter Adshead, John T. Giblin Jr, Mauro Pieroni, Zachary J. Weiner, Phys. Rev. Lett. 124, 171301 (2020), <https://arxiv.org/abs/1909.12843>
- [28] This is reminiscent of early works on the cosmological constant attributed to the vacuum-energy density of local field theories. Among them we mention the “vacuum-energy” density $\rho_{\Lambda}^{\text{vac}} \approx \pi/(2\ell_{\text{pl}}^2 H_0^{-2})$, rather than $\rho_{\Lambda}^{\text{vac}} \propto 1/(\ell_{\text{pl}}^4)$, V. G. Gurzadyan and S.-S. Xue, IJMPA 18 (2003) 561-568, astro-ph/0105245.
- [29] S.-S. Xue, IJMPA Vol. 24 (2009) 3865-3891, arXiv:hep-th/0608220
- [30] S.-S. Xue, Nuclear Physics B897 (2015) 326; Int. J. Mod. Phys. 30 (2015) 1545003, <https://arxiv.org/abs/1410.6152v3>
- [31] G. W. Gibbons and S. W. Hawking, Phys. Rev.D 15 (1977) 27382751.
L. Parker, Phys. Rev. Lett. 21562 (1968); Phys. Rev. 183, 1057 (1969); Phys. Rev. D3, 346 (1971);
L. Parker and D. J. Toms, Quantum field theory in curved spacetime: quantized fields and gravity, Cambridge University Press, Cambridge (2009);
N. D. Birrell and P. C. W. Davies, Quantum fields in curved space, Cambridge University Press, Cambridge (1982).
E. Mottola, Phys. Rev. D 31, 754 (1985).
S. Habib, C. Molina-Paris and E. Mottola, Phys. Rev. D61, 024010 (2000) [gr-qc/9906120].
P. R. Anderson and E. Mottola, Phys. Rev. D89, 104038 (2014) [arXiv:1310.0030 [gr-qc]]; Phys. Rev. D89, 104039 (2014) [arXiv:1310.1963 [gr-qc]].

- [32] L. H. Ford, Phys. Rev. D 35, 2955 (1987).
 D. J. H. Chung, P. Crotty, E. W. Kolb and A. Riotto, Phys. Rev. D 64, 043503 (2001) [hep-ph/0104100].
 Daniel J. H. Chung, Edward W. Kolb, Andrew J. Long, JHEP 01(2019)189,
<https://arxiv.org/abs/1812.00211>.
 Yohei Ema, Kazunori Nakayama, Yong Tang, JHEP 09(2018)135, <https://arxiv.org/abs/1804.07471>.
 S. Hashiba, Jun'ichi Yokoyama, Phys. Rev. D 99, 043008 (2019), <https://arxiv.org/abs/1812.10032>,
 and Phys. Lett. B 798, 135024 (2019), <https://arxiv.org/abs/1905.12423>
 Lingfeng Li, Tomohiro Nakama, Chon Man Sou, Yi Wang, Siyi Zhou, JHEP07(2019)067
<https://arxiv.org/pdf/1903.08842.pdf>
- [33] S.-S. Xue, “Cosmological Λ driven inflation and produced particles”, <http://arxiv.org/abs/1910.03938>
 the short letter “Cosmological constant, matter, cosmic inflation and coincidence”, Modern Physics
 Letters A, (2020) 2050123, DOI: 10.1142/S0217732320501230, <https://arxiv.org/abs/2004.10859>
- [34] S.-S. Xue, “Cosmological Λ converts to reheating energy and cold dark matter”,
<https://arxiv.org/abs/2006.15622>
- [35] J. Mielczarek, Phys. Rev. D83:023502, 2011, arXiv1009.2359.
- [36] Planck Collaboration, “Planck 2018 results. VI. Cosmological parameters”,
<https://arxiv.org/abs/1807.06209>
- [37] See for example, B. W. Lee and S. Weinberg Phys. Rev. Lett. 39, (1977); R. Ruffini, J. D. Salmonson,
 J. R. Wilson and S.-S. Xue, A&A 350, 334(1999)343, 359(2000) 855.
- [38] A. A. Starobinsky, Phys. Lett. B 91 (1980) 99.
- [39] S. Hollands and R. Wald, *Gen. Rel. Grav.* 34 (2002) 2043-2055, arXiv:gr-qc/0205058
- [40] J. J. Sakurai, *Modern Quantum Mechanics*, Addison Wesley (Reading, MA, 1994).
- [41] L.D. Landau and E.M. Lifshiz, “Quantum Mechanics” (Non-relativistic Theory), Elsevier Butterworth-
 Heinemann ISBN 0 7506 3539 8
- [42] A. D. Sakharov, “Violation of CP invariance, C asymmetry, and baryon asymmetry of the universe”.
 Journal of Experimental and Theoretical Physics Letters. 5: 2427 (1967).